Chemical Geology 557 (2020) 119856

Contents lists available at ScienceDirect

Chemical Geology

journal homepage: www.elsevier.com/locate/chemgeo

# Thallium isotope ratios in shales from South China and northwestern Canada suggest widespread $O_2$ accumulation in marine bottom waters was an uncommon occurrence during the Ediacaran Period

Chadlin M. Ostrander[a,b,c,*], Jeremy D. Owens[d], Sune G. Nielsen[c,e], Timothy W. Lyons[f], Yunchao Shu[c,g], Xinming Chen[d], Erik A. Sperling[h], Ganqing Jiang[i], David T. Johnston[j], Swapan K. Sahoo[i,k], Ariel D. Anbar[a,l]

[a] School of Earth and Space Exploration, Arizona State University, Tempe, AZ 85287, USA
[b] Department of Marine Chemistry and Geochemistry, Woods Hole Oceanographic Institution, Woods Hole, MA 02543, USA
[c] NIRVANA Laboratories, Woods Hole Oceanographic Institution, Woods Hole, MA 02543, USA
[d] Department of Earth, Ocean, and Atmospheric Science, National High Magnetic Field Laboratory, Florida State University, Tallahassee, FL 32306, USA
[e] Department of Geology and Geophysics, Woods Hole Oceanographic Institution, Woods Hole, MA 02543, USA
[f] Department of Earth and Planetary Sciences, University of California, Riverside, CA 92521, USA
[g] CAS Key Laboratory of Crust-Mantle Materials and Environments, School of Earth and Space Sciences, University of Science and Technology of China, Hefei, Anhui 230026, China
[h] Department of Geological Sciences, Stanford University, Stanford, CA 94305, USA
[i] Department of Geoscience, University of Nevada, Las Vegas, NV 89154, USA
[j] Department of Earth and Planetary Science, Harvard University, Cambridge, MA 02138, USA
[k] Equinor US, Houston, TX, USA
[l] School of Molecular Sciences, Arizona State University, Tempe, AZ 85287, USA

ARTICLE INFO

Editor: Michael E. Boettcher

*Keywords:*
Thallium
Isotopes
Ediacaran
Oxygen
Redox
Ediacaran Biota
Mn oxides

ABSTRACT

The tempo and magnitude of ocean oxygenation during the rise of animals in the Ediacaran Period (635 to 539 million years ago, or Ma) is debated. Reconciling this debate is key to understanding what role, if any, oxygen played in the rise of large morphologically complex life on Earth. We reconstruct a portion of Ediacaran ocean oxygenation history using thallium isotope records (reported as $\varepsilon^{205}Tl$) captured in shales from South China (Wuhe section) and northwestern Canada (Goz A and Sekwi Brook sections). At first blush, our $\varepsilon^{205}Tl$ data from these two locations are very different. South China shales reveal two pronounced and extremely negative Tl isotope excursions, in mid-members II and III of the Doushantuo Formation (where $\varepsilon^{205}Tl_{authigenic}$ reach nadirs of $-10.4 \pm 0.2$; 2SD and $-9.1 \pm 0.2$; 2SD, respectively). In contrast, northwestern Canada shales reveal fairly invariant values (average $\varepsilon^{205}Tl_{authigenic} = -2.1 \pm 1.6$; 2SD, n = 75). These disparate records are in much better agreement, however, if we cull from our dataset shales that were inferred in previous work to have been deposited in restricted settings. By comparison to analogous modern settings (e.g., the Black Sea), $\varepsilon^{205}Tl$ data in these shales most likely fingerprint local-scale processes. On the other hand, and also by comparison to modern settings (e.g., Cariaco and Santa Barbara basins), shales deposited in an open ocean setting probably captured a globally homogenous seawater $\varepsilon^{205}Tl$ ($\varepsilon^{205}Tl_{SW}$). Moving forward with this assumption, we find that Ediacaran open ocean $\varepsilon^{205}Tl_{SW}$ values were predominantly comparable to bulk upper continental crust ($\varepsilon^{205}Tl = \sim -2$). These relatively heavy open ocean $\varepsilon^{205}Tl_{SW}$ imply limited Mn oxide burial in global marine sediments for large periods of time during the Ediacaran, and by inference also limited accumulation of $O_2$ in global marine bottom waters. Only for what appear to be very brief episodes of time (≪5–10 million years) at ~635 Ma and ~580 Ma did open ocean $\varepsilon^{205}Tl_{SW}$ reach values considerably lighter than bulk upper continental crust (for example, $\varepsilon^{205}Tl_{SW}$ as low as $-4.4 \pm 0.2$; 2SD at ~635 Ma and $-5.3 \pm 0.3$: 2SD at ~580 Ma). These much rarer negative $\varepsilon^{205}Tl_{SW}$ values require short-lived episodes of globally enhanced Mn oxide burial in marine sediments, and by implication also brief episodes of enhanced accumulation of $O_2$ in global marine bottom waters. When interpreting geochemical data, it is important to make global-scale inferences only after identifying and accounting for local-scale overprints. Applying this strategy ourselves, we find compelling evidence for an

* Corresponding author at: Department of Marine Chemistry and Geochemistry, Woods Hole Oceanographic Institution, Woods Hole, MA 02543, USA.
*E-mail address:* costrander@whoi.edu (C.M. Ostrander).

https://doi.org/10.1016/j.chemgeo.2020.119856
Received 26 May 2020; Received in revised form 24 August 2020; Accepted 26 August 2020
Available online 27 August 2020

Ediacaran global ocean that only very briefly experienced widespread bottom water oxygenation during the rise of animals.

## 1. Introduction

Constraining the history of ocean oxygenation during the Ediacaran Period (635 to 539 million-years-ago, or Ma) has been difficult. Some of the uncertainty stems from fingerprints of widespread ocean oxygenation that are found in some sedimentary rocks deposited during the Ediacaran but not in others of roughly the same age. For instance, redox-sensitive elements (RSEs; e.g., V, Cr, Mo, Re, and U) are at times highly enriched in shales and pyrite from South China and have been treated as evidence for widespread Ocean Oxygenation Events ("OOEs" (Scott et al., 2008; Sahoo et al., 2012, 2016; Gregory et al., 2017)). Strong shale RSE enrichments can fingerprint widespread ocean oxygenation because accumulation of RSEs in seawater, and by extension also in coeval marine sediments worldwide, should scale to first order with levels of global ocean oxygenation (Scott et al., 2008; Partin et al., 2013; Reinhard et al., 2013; Sahoo et al., 2016; Sheen et al., 2018). The OOE hypothesis, however, is complicated by the absence of pronounced RSE enrichments in roughly coeval shales from northwestern Canada (Johnston et al., 2013; Sperling et al., 2016; Miller et al., 2017). Reconciling the differences in these records is crucial if we are to understand what role, if any, marine oxygenation played in promoting the rise of complex life during the Ediacaran (Sperling et al., 2015a; Cole et al., 2020).

Some disparities between these two shale RSE records must be due to local-scale differences at the time of deposition. Shales from both locations are thought to have been deposited almost exclusively under a locally anoxic water column. However, South China shales were deposited primarily under $H_2S$-bearing ("euxinic") conditions (e.g., Li et al., 2010; Sahoo et al., 2016), while the shales of northwestern Canada reflect $Fe^{2+}$-rich ("ferruginous") depositional conditions (e.g., Johnston et al., 2013; Sperling et al., 2016). Whether a shale was deposited under $H_2S$-rich or $Fe^{2+}$-rich anoxic conditions plays a key role in its ability to accumulate RSEs (Tribovillard et al., 2006; Bennett and Canfield, 2020). Second, it was recently proposed that RSE delivery to the South China shales was supplemented by some combination of (a) short-term changes in local redox conditions and (b) the operation of a local manganese (Mn) oxide "shuttle" (Ostrander et al., 2019a). Neither process has been proposed during deposition of shales from northwestern Canada. Third, it was also suggested in Ostrander et al. (2019a) that the transient nature of the RSE enrichments in South China shales was due at least in part to changes in the strength of connection of the paleo-basin to the open ocean. Changes in basin connectivity have not been invoked during deposition of roughly coeval shales from northwestern Canada. Finally, Ediacaran-aged shales from some sections in South China may be highly condensed compared to their northwestern Canada counterparts. The condensed nature of South China sections would likely accentuate RSE enrichments (discussed also in Miller et al., 2017). In sum, there are multiple local-scale parameters that must be considered when comparing data from these shales if the goal is to evaluate the presence or absence of global-scale trends.

Here, we use thallium (Tl) isotopes in an attempt to see through these local-scale overprints and, when possible, infer the tempo and magnitude of Ediacaran global ocean oxygenation. We have generated Tl isotope data for 60 shale samples from South China (Wuhe section) and 75 shale samples from northwestern Canada (Goz A and Sekwi Brook sections). We have targeted the same shale samples that host the conflicting RSE records discussed above (that is, shales investigated previously in Johnston et al., 2013; Sperling et al., 2016; and Sahoo et al., 2012, 2016).

Thallium isotopes are emerging as a powerful tool for tracking Earth's ocean oxygenation history (Nielsen et al., 2011; Ostrander et al., 2017, 2019b; Them et al., 2018; Bowman et al., 2019; Fan et al., 2020). Thallium possesses an affinity for Mn oxide minerals, and once sorbed to their surfaces and subsequently oxidized from $Tl^+$ to $Tl^{3+}$ will undergo substantial positive isotope fractionation (particularly after sorption to hexagonal birnessite (Peacock and Moon, 2012; Nielsen et al., 2013)). Manganese oxides are ubiquitous on the seafloor today because their formation and subsequent preservation is dependent on $O_2$, which is abundant in marine bottom waters throughout the oceans. The widespread occurrence of Mn oxides today, and the concomitant preferential removal of the heavier-mass Tl isotope from seawater, drives the globally homogenous seawater Tl isotope composition ($\varepsilon^{205}Tl_{SW}$) to a lighter value compared to oceanic inputs ($\varepsilon^{205}Tl_{SW} = -6.0 \pm 0.3$; 2SD (Nielsen et al., 2006; Owens et al., 2017) versus $\varepsilon^{205}Tl_{IN} = \sim -1.8$ (Nielsen et al., 2017); summarized in Fig. 1). This $\varepsilon^{205}Tl_{SW}$ is captured and preserved in organic-rich marine sediments today deposited under anoxic bottom waters, presumably because of quantitative Tl removal from marine bottom waters in these settings (Owens et al., 2017). Important for this study, capture of $\varepsilon^{205}Tl_{SW}$ in anoxic settings seems to occur irrespective of $H_2S$ availability. For example, $\varepsilon^{205}Tl_{SW}$ is captured in sediments today in the Cariaco Basin where $H_2S$ is present in bottom waters (Owens et al., 2017) and is also captured in sediments in the Santa Barbara Basin where $H_2S$ is limited strictly to pore waters (Fan et al., 2020). By analogy with today, past $\varepsilon^{205}Tl_{SW}$ should have been governed by the global extent of bottom water ocean oxygenation (as scaled to associated Mn oxide burial) and captured in organic-rich marine sediments deposited under anoxic conditions. As proof of concept, Tl isotopes in shales deposited under anoxic conditions have successfully been used to track widespread marine bottom water oxygenation (Ostrander et al., 2019b; Fan et al., 2020) and deoxygenation (Nielsen et al., 2011; Ostrander et al., 2017; Them et al., 2018; Bowman et al., 2019) at various times in Earth's past.

Critically, open ocean $\varepsilon^{205}Tl_{SW}$ values are shown to be captured in sediments in anoxic settings today only when they are well connected to the open ocean. The surface water $\varepsilon^{205}Tl$ is still captured in sediments deposited well below the chemocline in the one strongly restricted basin investigated to date (the Black Sea), but this $\varepsilon^{205}Tl$ signal

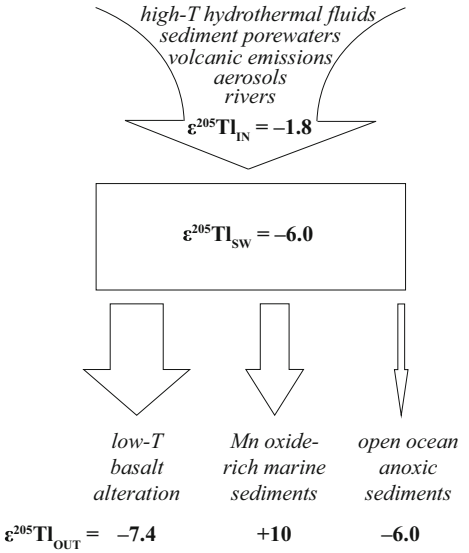


**Fig. 1.** Modern seawater Tl isotope mass-balance. See Table 2 for accompanying references and notes.

differs markedly from that of the open ocean ($\varepsilon^{205}Tl = -2.2 \pm 0.3$; 2SD (Owens et al., 2017)). This $\varepsilon^{205}Tl_{SW}$ difference probably occurs because delivery of Tl to the Black Sea is dominated by local river inputs (presumably with $\varepsilon^{205}Tl = \sim -2$; Nielsen et al., 2005), and not open-ocean seawater as is likely the case in the Cariaco Basin (Owens et al., 2017). The critical take-home message here is that use of Tl isotopes as a global proxy demands deposition in settings that are not strongly restricted.

## 2. Ediacaran shale samples

### 2.1. South China shales

Shales from the Doushantuo Formation used in this study were collected from the Wuhe section in Guizhou Province, South China (Fig. 2). Fresh shale slabs were originally collected from river-cut outcrops for the purposes of bulk and trace element analyses, iron (Fe) speciation, and sulfur (S) isotopes (Sahoo et al., 2012, 2016). Throughout South China, the Doushantuo Formation has been split into four distinct members (summarized in Jiang et al., 2011). As for the remainder of the Yangtze Platform, Member I at the Wuhe site is comprised of cap carbonates that overly diamictites associated with the Marinoan Glaciation. Throughout the rest of the Doushantuo at Wuhe, organic-rich black shales are the dominant lithology (extending over 10s of meters in mid-Members II and III), but these shales are frequently interrupted by intervals of carbonate deposition. Carbonate beds are most frequent at the base of Members II and III and also at the top of Member III. Zircon U–Pb ages from volcanic ash beds in Member I (635.2 ± 0.6 Ma) and what had been inferred at the time as uppermost Member IV (551.1 ± 0.7 Ma) of the Doushantuo Formation were thought to constrain its duration to ~84 million years (myr) into the Ediacaran Period (Condon et al., 2005). It was later suggested,

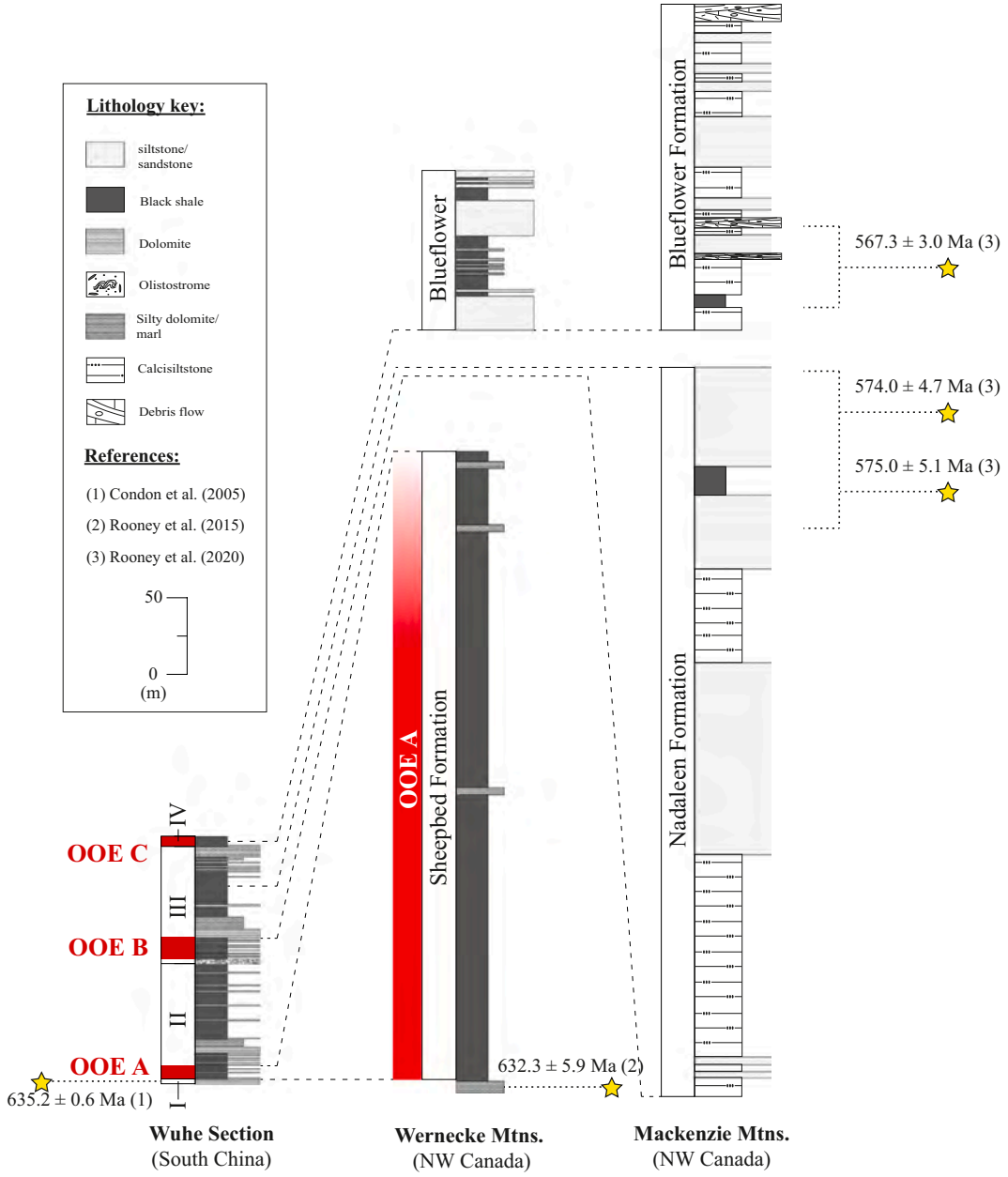


**Fig. 2.** Stratigraphic columns for the sections targeted in this study. Stratigraphy for the Wuhe section is modified from Jiang et al. (2011), for the Wernecke Mountains section is modified from Johnston et al. (2013), and for the Mackenzie Mountains section is modified from Sperling et al. (2016). Available geochronological constraints from elsewhere in the Rackla Group outcrop belt and stratigraphic correlations have been included (see the text and legend box for references).

however, based on alternative inferences of stratigraphic correlations in South China, that the Doushantuo Formation did not extend this far into the Ediacaran, perhaps only to ≥560 Ma (An et al., 2015). Recently reported Re–Os ages for mid- to late-Ediacaran shales in Oman and northwest Canada would suggest, via chemostratigraphic correlation, an age estimate of ~565 Ma for Doushantuo Member IV, and thus may also support this refined age estimation (Rooney et al., 2020). In either case, the Doushantuo Formation is very thin stratigraphically at the Wuhe site given how much geologic time it is thought to represent (≥75 to 85 myr preserved in ~120 m of stratigraphy; see Fig. 2). It is possible that the Wuhe section may be extremely condensed (discussed in Miller et al., 2017), or unconformities within the section may have been overlooked (or some combination of the two).

The Wuhe site, more generally, preserves Ediacaran sedimentary rocks deposited below wave base in a slope setting within the Nanhua paleo-basin (summarized in Jiang et al., 2011). Classically, the paleo-slope is thought to have maintained a strong and uninterrupted connection with the open ocean (e.g., Sahoo et al., 2012, 2016). More recently, however, it has been suggested based on multiple independent lines of evidence that this slope instead may not have maintained a consistently strong connection with the open ocean (e.g., as suggested by inferred changes in sea level and their relationships with some geochemical trends (Ostrander et al., 2019a)). Instead, Ostrander et al. (2019a) argued that these shales may have been deposited for long periods of time during the Ediacaran in a semi-restricted marine basin. Such a scenario could have favored the frequent euxinia suggested for the Doushantuo Formation based on Fe speciation data (e.g., Li et al., 2010; Sahoo et al., 2012, 2016). Restricted settings favor euxinic conditions today (e.g., the Black Sea), although levels of restriction need not be extreme (e.g., Cariaco Basin). These hypotheses are in agreement with Och et al. (2016), who compiled geochemical data from many sedimentary sections in South China and speculated that the Ediacaran Nanhua Basin was comprised of a series of successive restricted waterways. The conclusion of Ostrander et al. (2019a), specifically the notion of a restricted waterway for the depositional site of the Wuhe section, is therefore an extension of this model. If correct, this inferred setting carries important implications for the application of some geochemical proxies, including Tl isotopes.

### 2.2. Northwestern Canada shales

Our shales from northwestern Canada were collected at two sites: the Goz A section in the Wernecke Mountains and the Sekwi Brook section in the Mackenzie Mountains (Fig. 2). In stratigraphic order, both sections cover the Sheepbed Formation, Nadaleen Formation, Gametrail Formation, Blueflower Formation, and the Risky Formation (together comprising the Rackla Group). Of note, the Nadaleen Formation was only recently formalized (Moynihan et al., 2019) and was informally referred to as the June Beds in previous publications (Macdonald et al., 2013; Johnston et al., 2013; Sperling et al., 2016). Also of note, the Gametrail Formation hosts the large negative carbonate carbon isotope excursion known as the Shuram Carbon Isotope Excursion (CIE (Macdonald et al., 2013; Moynihan et al., 2019)). Shales were only sampled from the shale-rich Sheepbed, Nadaleen, and Blueflower formations, and, as for the South China shales, these shale samples were collected from fresh outcrops for bulk and trace element analyses, Fe speciation, and S isotopes (see Johnston et al., 2013; Sperling et al., 2016). The oldest samples we targeted from northwestern Canada are from the Sheepbed Formation (analyzed only from Goz A), which was deposited shortly after the end of the Marinoan Glaciation based on a shale Re–Os age near its base of 632.3 ± 5.9 Ma (Rooney et al., 2015) and its stratigraphic position directly above distinctive Marinoan cap carbonates. We targeted shales from the younger Nadaleen Formation at Sekwi Brook, which was deposited around ~575 Ma based on a recent Re–Os age (Rooney et al., 2020). The youngest shales we targeted from northwestern Canada, from both sites, are from the Blueflower Formation, which was deposited around 567.3 ± 3.0 Ma based on another recent Re–Os age (Rooney et al., 2020). Ediacaran strata from our two northwestern Canada sites are thicker than their inferred coeval equivalents in South China, extending hundreds of meters more despite preserving a much shorter time window (see Fig. 2 for a side-by-side comparison).

Shales from our northwestern Canada sites were likely deposited in different environmental settings depending on locality and time, with Goz A representing a more proximal setting compared to Sekwi Brook (Macdonald et al., 2013). The Sheepbed Formation at Goz A consists of black shales interbedded with thin, micritic limestones, and represents basinal shales deposited below storm wave base (likely near the shelf-slope break) during transgression following the Marinoan glaciation. The Blueflower Formation at Goz A was deposited in shallower conditions and consists of a mixture of shale, siltstone and sandstone deposited in inner- to outer-shelf environments. In contrast, Sekwi Brook records a persistent deep-water slope environment. Both the Nadaleen and Blueflower formations here are comprised of a heterolithic mixture of black shales, micritic limestone, siltstone and calcisiltstone, and rarer coarser-grained intervals. Both formations do record gravity-flow deposits (turbidites and debrites; Dalrymple and Narbonne, 1996; Macdonald et al., 2013), but care was taken to only sample background hemipelagic shales that were deposited relatively slowly. Unlike their coeval equivalents from South China, shales from northwestern Canada were probably not frequently deposited in restricted settings. Consistent with this assumption, Fe speciation data in northwestern Canada shales indicate deposition under predominantly ferruginous conditions (Canfield et al., 2008; Johnston et al., 2013; Sperling et al., 2015b), which are the conditions thought to dominate the Proterozoic deep ocean (Poulton and Canfield, 2011; Planavsky et al., 2011).

### 2.3. Stratigraphic correlations

We adopt the Ediacaran stratigraphic correlations proposed in Macdonald et al. (2013) (see Fig. 2). The strongest temporal link between our study sites is based on geochronological constraints that show agreement within error from zircon collected from Doushantuo Formation Member I (a U–Pb age of 635.2 ± 0.6 Ma (Condon et al., 2005)) and shales in the lowermost Sheepbed Formation (a Re–Os age of 632.3 ± 5.9 Ma (Rooney et al., 2015)). The distinctive Marinoan cap carbonates (Ravensthroat and Hayhook formations) directly underlying the Sheepbed Formation are also clearly correlative with Doushantuo Member I on lithostratigraphic grounds. Adopting this correlation equates our Sheepbed Formation samples (Wernecke Mountains) to lowermost Member II of the Doushantuo Formation and therefore also to the time of the oldest purported Ediacaran OOE (OOE A). Outside of this one strong tie-point, correlations are much more difficult and based only on trends in the putative global carbonate carbon isotope record during the Ediacaran (again, see Macdonald et al., 2013). Based on the presence of the Shuram CIE in the Gametrail Formation in northwestern Canada (Macdonald et al., 2013; Moynihan et al., 2019; Rooney et al., 2020), we can equate the Nadaleen Formation samples to the pre-Shuram CIE stratigraphy of the Doushantuo Formation, specifically mid-Member III (Jiang et al., 2011). It is currently impossible to be more specific than “pre-Shuram” in this case because there are questions about where, if at all, the Shuram CIE is expressed in the Wuhe section (Jiang et al., 2007, 2011). Finally, both sets of Blueflower Formation samples are then roughly equivalent to the post-Shuram CIE stratigraphy of the Doushantuo Formation, specifically lower- to mid-Member IV and extending beyond its terminus (Jiang et al., 2011). This final correlation may suggest that OOE C, which occurs during deposition of Member IV, overlaps with some Blueflower Formation stratigraphy. However, while there is almost certainly correlation between the lower Sheepbed Formation and lower Doushantuo Member II during hypothesized OOE-A, and available data allow for reasonable correlation of pre- and post-Shuram CIE

stratigraphic packages, sample-to-sample correlations between the Nadaleen and Blueflower formations and the Doushantuo Formation are not possible at this point.

Our shales from northwestern Canada were deposited a great distance from their South China equivalents throughout the Ediacaran according to recent paleogeographic reconstructions (Li et al., 2013 and references therein; Fig. 3). Our sample set therefore provides us with a unique opportunity to discern local- from global-scale changes in ocean redox conditions during this period in Earth history.

## 3. Tl isotope methods

Shale samples from Wuhe and Sekwi Brook were crushed in a tungsten carbide shatterbox, and those from Goz A were crushed in a hardened steel shatterbox. Once in powder form, all subsequent sample preparation and purification steps were performed in the NIRVANA Laboratory at Woods Hole Oceanographic Institution (WHOI) and the National High Magnetic Field Laboratory (NHMFL) at Florida State University (FSU), following methods outlined in previous work (Rehkämper and Halliday, 1999; Nielsen et al., 2004; Owens et al., 2017). Powdered samples were first transferred to Teflon reactors and treated with 2 M $HNO_3$ for 12 to 15 h at 130 °C, a treatment shown to effectively separate authigenic Tl bound to pyrite from detrital Tl (Nielsen et al., 2011). Following this partial dissolution, samples were centrifuged, and their supernatants containing the authigenic fraction were transferred by pipette to new Teflon reactors. Special care was taken to avoid disturbing the solid (detrital) residues during this step. If a residue was disturbed, samples were re-centrifuged prior to another

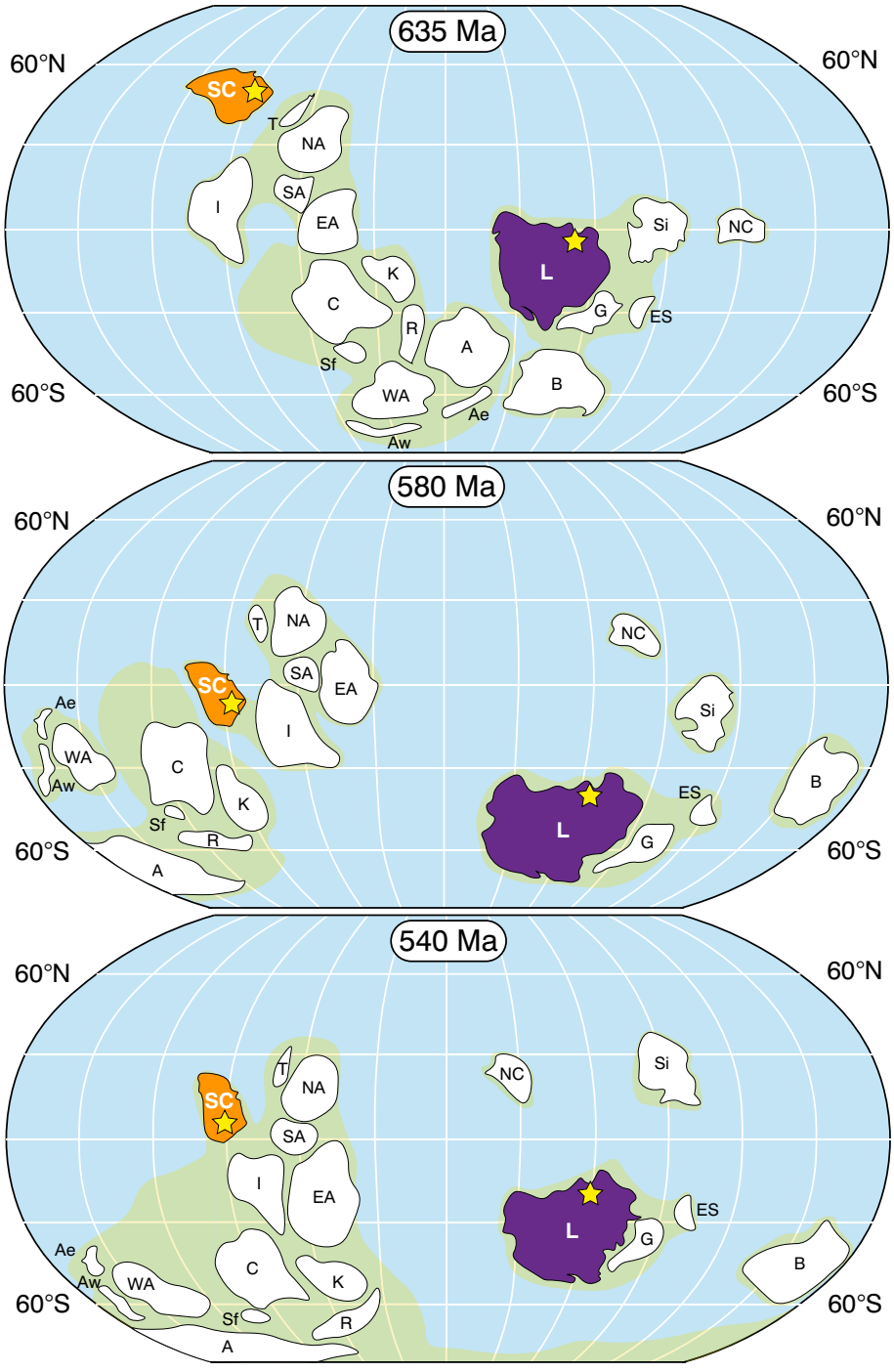


**Fig. 3.** Paleographic reconstructions at three different time-slices during the Ediacaran Period. Yellow stars signify rough estimates for the paleolocations of our South China (orange) and northwestern Canada (blue) study sites. Craton/terrane name abbreviations: A = Amazonia; Ae = Avalonia (east); Aw = Avalonia (west); B = Baltica; C = Congo; EA = East Antarctica; ES = East Svalbard; G = Greenland; I = India; K = Kalahari; L = Laurentia; NA = Northern Australia; NC = North China; R = Rio Plata; SA = Southern Australia; SC = South China; Sf = Sao Francisco; Si = Siberia; T = Tarim; WA = West Africa. (For interpretation of the references to color in this figure legend, the reader is referred to the web version of this article.)
Figure based on the reconstructions of Li et al. (2013).

transfer attempt. After centrifugation, all authigenic fractions, and some detrital fractions from the South China samples, were digested for 1.5 h at ~300 °C and 100 bar in a high-pressure asher (WHOI) or by microwave (FSU) to dissolve organic compounds. After dissolution of the South China detrital residues in 1:1 concentrated $HNO_3$ and HF, these detrital fractions and all of the authigenic fractions were then completely dissolved in 1 M HCl in preparation for Tl purification via ion-exchange chromatography. Because our authigenic fractions were never treated with HF, even if some detrital material had been incorrectly transferred during the leach step it would not be expected to dissolve. A visual check of all authigenic fractions was also conducted prior to chromatography to check for incorrectly transferred detrital residue. Similar to the approach taken in Ostrander et al. (2017), each authigenic fraction was passed through one micro-column. Because the Tl:matrix ratios were much lower for the South China detrital fractions, however, each of these was first passed through a large glass column and then a micro-column to remove the additional matrix.

Thallium isotope analyses were conducted at the WHOI Plasma Mass Spectrometry Facility and at the NHMFL. At both locations, a Thermo Neptune multi-collector inductively coupled plasma mass spectrometer (MC-ICPMS) was used with an Aridus II desolvating nebulizer sample introduction system. Measurements were made in low-resolution mode using sample-standard bracketing relative to NIST 997 Tl in epsilon notation. Instrumental mass bias was monitored using external normalization to NIST SRM 981 Pb. Because each sample was doped with a known quantity of NIST SRM 981 Pb, Tl concentrations could be calculated during MC-ICPMS analysis using the measured $^{205}Tl/^{208}Pb$ ratios. We report all Tl isotope values in epsilon notation relative to NIST 997 Tl metal:

$$\varepsilon^{205}Tl = \left(\frac{^{205/203}Tl_{sample}}{^{205/203}Tl_{NIST-997}} - 1\right) \times 10{,}000.$$

At least one USGS shale SCo-1 standard was leached, purified, and analyzed with each sample set to monitor accuracy (Table 1). Measured $\varepsilon^{205}Tl_{authigenic}$ for SCo-1 powders from vials housed at WHOI ($\varepsilon^{205}Tl = -3.0 \pm 0.2$; 2SD, n = 4) and FSU ($\varepsilon^{205}Tl = -3.1 \pm 0.6$; 2SD, n = 2) were within error of one another and reproduced values reported in a recent study (Ostrander et al., 2017, where the same WHOI SCo-1 vial yielded $\varepsilon^{205}Tl_{authigenic} = -2.9 \pm 0.1$; 2SD, n = 9). However, authigenic $\varepsilon^{205}Tl$ for SCo-1 powders from a vial housed at Arizona State University were slightly different ($\varepsilon^{205}Tl = -3.4 \pm 0.2$; 2SD, n = 9), even though these standards were prepared alongside those from the WHOI vial. It is plausible that these slight differences were due to previously unrecognized heterogeneities in $\varepsilon^{205}Tl_{authigenic}$ between SCo-1 vials. In contrast, measured detrital $\varepsilon^{205}Tl$ between the SCo-1 vials from ASU ($\varepsilon^{205}Tl = -2.6 \pm 0.2$; 2SD, n = 4) and WHOI ($\varepsilon^{205}Tl = -2.5 \pm 0.4$; 2SD, n = 2) were within error of one another. These detrital $\varepsilon^{205}Tl$ data also matched values reported in Ostrander et al. (2017) (where SCo-1 $\varepsilon^{205}Tl_{detrital} = -2.5 \pm 0.3$; 2SD, n = 9). Guided by these SCo-1 data, all errors reported in this study for our shales represent the 2SD reproducibility of that sample or the 2SD reproducibility of the associated SCo-1 fraction processed alongside that sample, whichever is greater (summarized in Table 1).

## 4. Results

### 4.1. South China

The most striking feature of our dataset is two pronounced negative $\varepsilon^{205}Tl_{authigenic}$ excursions in shales from the Doushantuo Formation, one in the middle of Member II (to as low as $\varepsilon^{205}Tl_{authigenic} = -10.4 \pm 0.2$ at 38.8 m) and another in the middle of Member III (to as low as $\varepsilon^{205}Tl_{authigenic} = -9.1 \pm 0.2$ at 97.3 m) (Fig. 4). Measured $\varepsilon^{205}Tl_{authigenic}$ outside these excursions, which includes shale samples deposited during the purported OOEs, are less negative and comparatively invariant. For example, $\varepsilon^{205}Tl_{authigenic}$ values in lowermost Member II (0.0 m to 11.4 m) are all between $-4.2 \pm 0.2$; 2SD and $-2.0 \pm 0.5$; 2SD. In uppermost Member II and lowermost Member III (47.8 m to 82.2 m), $\varepsilon^{205}Tl_{authigenic}$ data are all between $-5.3 \pm 0.3$; 2SD and $-2.2 \pm 0.3$; 2SD. In Member IV (112.2 m to 117.7 m), values for $\varepsilon^{205}Tl_{authigenic}$ are all between $-3.5 \pm 0.2$; 2SD and $0.4 \pm 0.7$; 2SD. Authigenic shale Tl concentrations peak during the purported OOEs (approaching 3 μg/g).

Similar negative excursions are not revealed in the $\varepsilon^{205}Tl_{detrital}$ data, which are comparatively invariant (average $\varepsilon^{205}Tl_{detrital} = -3.6 \pm 1.9$; 2SD; Fig. 5). Notably, samples with lighter $\varepsilon^{205}Tl_{detrital}$ also possess increasingly lighter $\varepsilon^{205}Tl_{authigenic}$ ($R^2 = 0.8$). Detrital Tl concentrations are also enriched in shales deposited during the OOEs, but the magnitude of enrichment is about an order of magnitude lower than authigenic counterparts (~0.4 μg/g).

### 4.2. Northwestern Canada

Measured $\varepsilon^{205}Tl_{authigenic}$ in the overwhelming majority of shales from northwestern Canada, from both Goz A (Fig. 6) and Sekwi Brook (Fig. 7), are within error of bulk upper continental crust ($\varepsilon^{205}Tl_{BUCC} = -2.1 \pm 0.3$ (Nielsen et al., 2005)). The only notable deviation away from bulk crust $\varepsilon^{205}Tl$ is a slight negative $\varepsilon^{205}Tl_{authigenic}$ excursion in the lower Sheepbed Formation (Goz A) that reaches a nadir of $\varepsilon^{205}Tl_{authigenic} = -4.4 \pm 0.2$; 2SD. Authigenic Tl concentrations are low and invariant in all shales from northwestern Canada (maximum $Tl_{authigenic} = 0.3$ μg/g).

## 5. Discussion

We begin by first discussing the negative $\varepsilon^{205}Tl_{authigenic}$ excursions found in the Doushantuo Formation (South China) (Section 5.1). This text is then followed by a discussion of our comparatively invariant northwestern Canada $\varepsilon^{205}Tl_{authigenic}$ record (Section 5.2). Lastly, we finish by discussing the potential connections between our new shale Tl isotope record and global ocean oxygenation levels during the Ediacaran Period (Section 5.3).

### 5.1. Negative $\varepsilon^{205}Tl$ excursions in the Doushantuo Formation

There appear to be two distinct Tl sources in our South China shales. The primary Tl source in our shales was released during the initial leach

**Table 1**
Tl isotope data for USGS shale SCo-1.

| | $\varepsilon^{205}Tl_{authigenic}$ [a,b] | N | $\varepsilon^{205}Tl_{detrital}$ [a,b] | N | Processed alongside |
|---|---|---|---|---|---|
| This study | | | | | |
| ASU vial | −3.4 ± 0.2 | 9 | −2.6 ± 0.2 | 4 | Wuhe section |
| WHOI vial | −3.0 ± 0.2 | 4 | −2.5 ± 0.4 | 2 | Wuhe and Goz A sections |
| FSU vial | −3.1 ± 0.6 | 3 | N/A | | Sekwi Brook section |
| Ostrander et al. (2017) | | | | | |
| WHOI vial | −2.9 ± 0.1 | 9 | −2.5 ± 0.3 | 9 | |

[a] Measured relative to NIST 997 Tl.
[b] All reported errors are 2SD of the standard reproducibility.

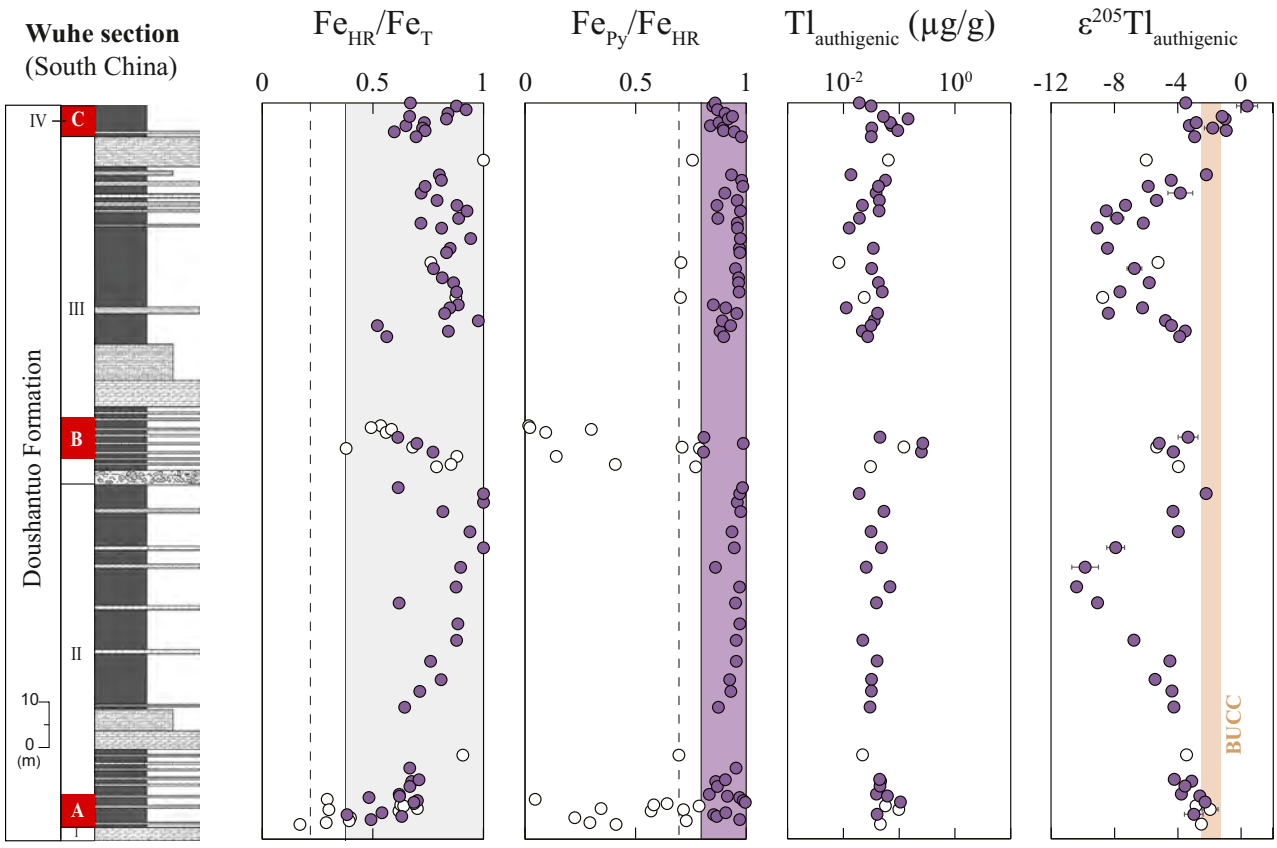


**Fig. 4.** Geochemistry of shales from the Wuhe section. Stratigraphy is modified from Jiang et al. (2011) and Fe speciation data and "OOE" intervals are from Sahoo et al. (2016). Purple circles signify samples deposited, according to Fe speciation data, under euxinic conditions ($Fe_{HR}/Fe_T \geq 0.38$ and $Fe_{Py}/Fe_{HR} \geq 0.80$ (Poulton and Canfield, 2011)). Dashed lines signify relaxed thresholds for anoxic and euxinic conditions ($Fe_{HR}/Fe_T \geq 0.22$ and $Fe_{Py}/Fe_{HR} \geq 0.70$ (Poulton and Canfield, 2011)). White circles signify shale samples deposited under non-euxinic conditions. The brown shaded region in the Tl isotope plot signifies the range of values for the bulk upper continental crust ($\varepsilon^{205}Tl_{BUCC} = -2.1 \pm 0.3$ (Nielsen et al., 2005)). (For interpretation of the references to color in this figure legend, the reader is referred to the web version of this article.)

step (i.e., $\varepsilon^{205}Tl_{authigenic}$; Fig. 4) and is responsible for our extremely negative isotope excursions. The subordinate Tl source in our shales was retained in our solid residues ($\varepsilon^{205}Tl_{detrital}$) and possesses a heavier, comparatively invariant Tl isotope composition (Fig. 5). A 100% successful leach should, in theory, result in a $\varepsilon^{205}Tl_{detrital}$ value comparable to the bulk upper continental crust ($\varepsilon^{205}Tl_{BUCC} = -2.1 \pm 0.3$ (Nielsen et al., 2005)). Given the predominance of authigenic Tl in our shales measured for both $\varepsilon^{205}Tl_{detrital}$ and $\varepsilon^{205}Tl_{authigenic}$ ($f_{authigenic} = 0.50$ to 0.89), and the likely difficulty associated with isolating 100% of the authigenic Tl during the leach step, it is unlikely that all of our leaches successfully removed 100% of the authigenic Tl. Thus, some of the authigenic fraction likely carried over to the detrital fraction. A good correlation between our measured $\varepsilon^{205}Tl_{detrital}$ and $\varepsilon^{205}Tl_{authigenic}$ supports this assumption ($R^2 = 0.8$; Fig. 5), suggesting isotopically light excess authigenic Tl was included in some of our detrital fractions. In theory, this correlation could also suggest that isotopically heavy detrital Tl was captured in some of our authigenic fractions. We argue that this alternative scenario is less likely, however, because detrital phases are less likely to dissolve in the dilute $HNO_3$ used during the leaching process. Furthermore, if any Tl from the solid (detrital) fraction was inadvertently transferred during the leach step to the authigenic fraction it would be unlikely to dissolve because HF was not used at any point during digestion of the authigenic fractions (discussed in Section 3).

#### 5.1.1. Unlikely links to global-scale processes

The two prominent negative $\varepsilon^{205}Tl_{authigenic}$ excursions found in the Doushantuo Formation—the largest found in shales of any age to date—could fingerprint dramatic perturbations to the global Tl cycle. The shale samples from the Wuhe section that host these excursions are thought, based on Fe speciation data (Sahoo et al., 2016; plotted in Fig. 4) and pyrite morphology (Wang et al., 2012), to have been deposited under a persistently euxinic water column. Accordingly, and by analogy with modern euxinic settings, these shales should have captured the overlying $\varepsilon^{205}Tl_{SW}$ during deposition (Owens et al., 2017). If these shales were deposited in a basin that maintained a strong connection to the open ocean (cf., Cariaco Basin), this $\varepsilon^{205}Tl_{SW}$ should have mirrored that of the open ocean. By extension, any variations to this $\varepsilon^{205}Tl_{SW}$ could then signify changes to past global Tl isotope mass-balance.

The only way to dramatically alter global Tl isotope mass-balance is to change the relative contribution of principal marine outputs for Tl (Baker et al., 2009). Although there is some isotopic heterogeneity in the Tl delivered to the ocean today, the overwhelming majority is isotopically indistinguishable from the bulk upper continental crust ($\varepsilon^{205}Tl_{IN} = \sim -1.8$; summarized in Nielsen et al. (2017), and also see Fig. 1). Second, two of the principal marine outputs for Tl are shown to impart significant isotope fractionation effects: low-temperature (low-T) alteration of oceanic crust (Nielsen et al., 2006) and highly oxidized Mn oxide-bearing marine sediments (Rehkämper et al., 2002; Nielsen et al., 2013). To further illustrate this concept, we employ the following isotope mass-balance equation:

$$\varepsilon^{205}Tl_{IN} = \varepsilon^{205}Tl_{OXIC}(f_{OXIC}) + \varepsilon^{205}Tl_{AOC}(f_{AOC}) + \varepsilon^{205}Tl_{ANOXIC}(f_{ANOXIC}), \quad (1)$$

where $\varepsilon^{205}Tl_X$ signifies the Tl isotope compositions of marine inputs

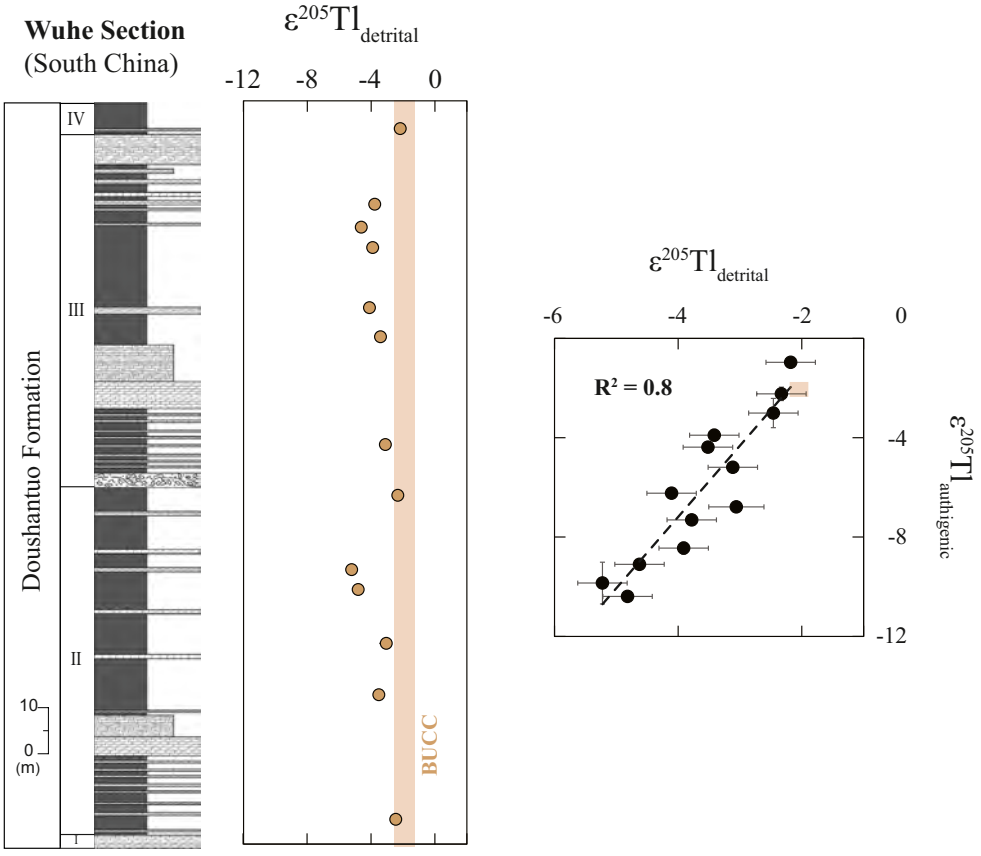


**Fig. 5.** Detrital Tl isotope data for shales from the Wuhe section. Stratigraphy is modified from Jiang et al. (2011). Accompanying cross-plot shows the general correlation between our measured detrital and authigenic Tl isotope compositions. The brown shaded regions in both plots signify the range of values for the bulk upper continental crust ($\varepsilon^{205}Tl_{BUCC} = -2.1 \pm 0.3$ (Nielsen et al., 2005)). (For interpretation of the references to color in this figure legend, the reader is referred to the web version of this article.)

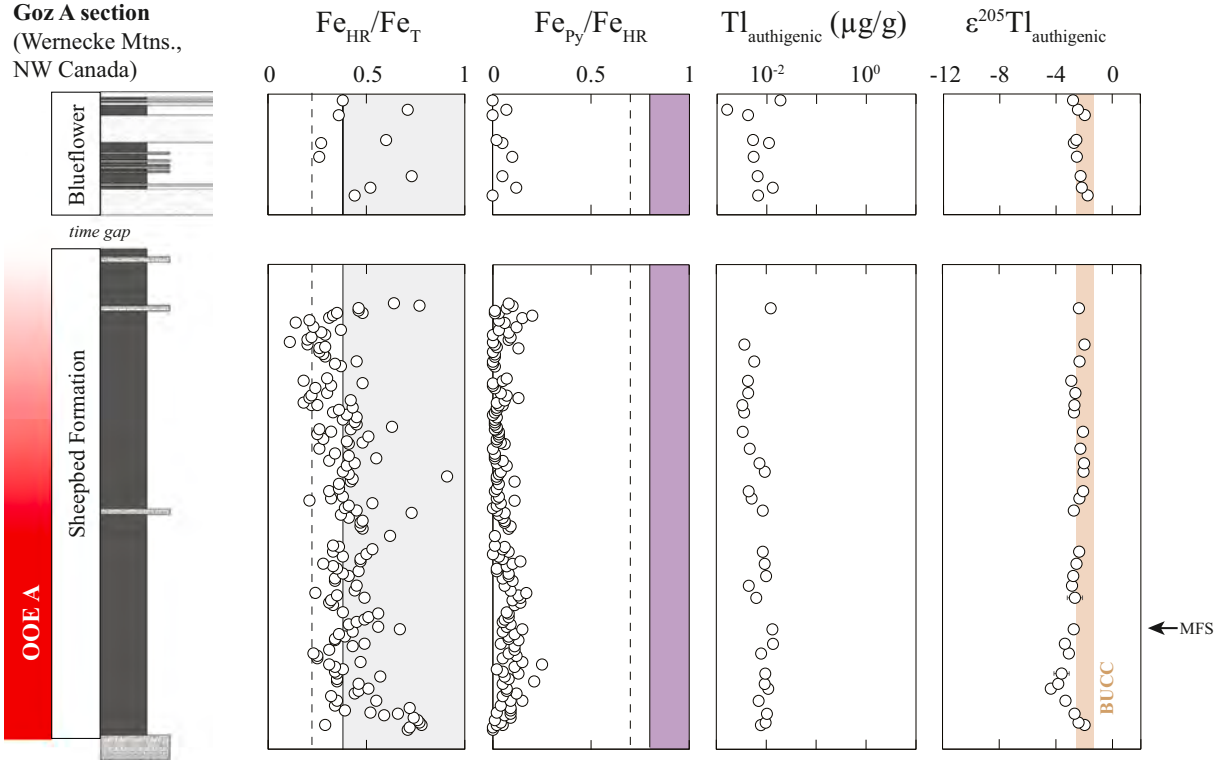


**Fig. 6.** Geochemistry of shales from the Goz A section. Stratigraphy is modified from Johnston et al. (2013) and Fe speciation data are from the same study. The grey and purple shaded areas signify the range of Fe speciation values indicative of anoxic ($Fe_{HR}/Fe_T \geq 0.38$) and euxinic ($Fe_{Py}/Fe_{HR} \geq 0.80$) local redox conditions, respectively (Poulton and Canfield, 2011). Dashed lines signify relaxed thresholds ($Fe_{HR}/Fe_T \geq 0.22$ and $Fe_{Py}/Fe_{HR} \geq 0.70$ (Poulton and Canfield, 2011)). White circles signify shale samples deposited under non-euxinic conditions (in this case, all samples). The brown shaded region in the Tl isotope plot signifies the range of values for the bulk upper continental crust ($\varepsilon^{205}Tl_{BUCC} = -2.1 \pm 0.3$ (Nielsen et al., 2005)). "MFS" refers to a maximum flooding surface identified in Johnston et al. (2013). (For interpretation of the references to color in this figure legend, the reader is referred to the web version of this article.)

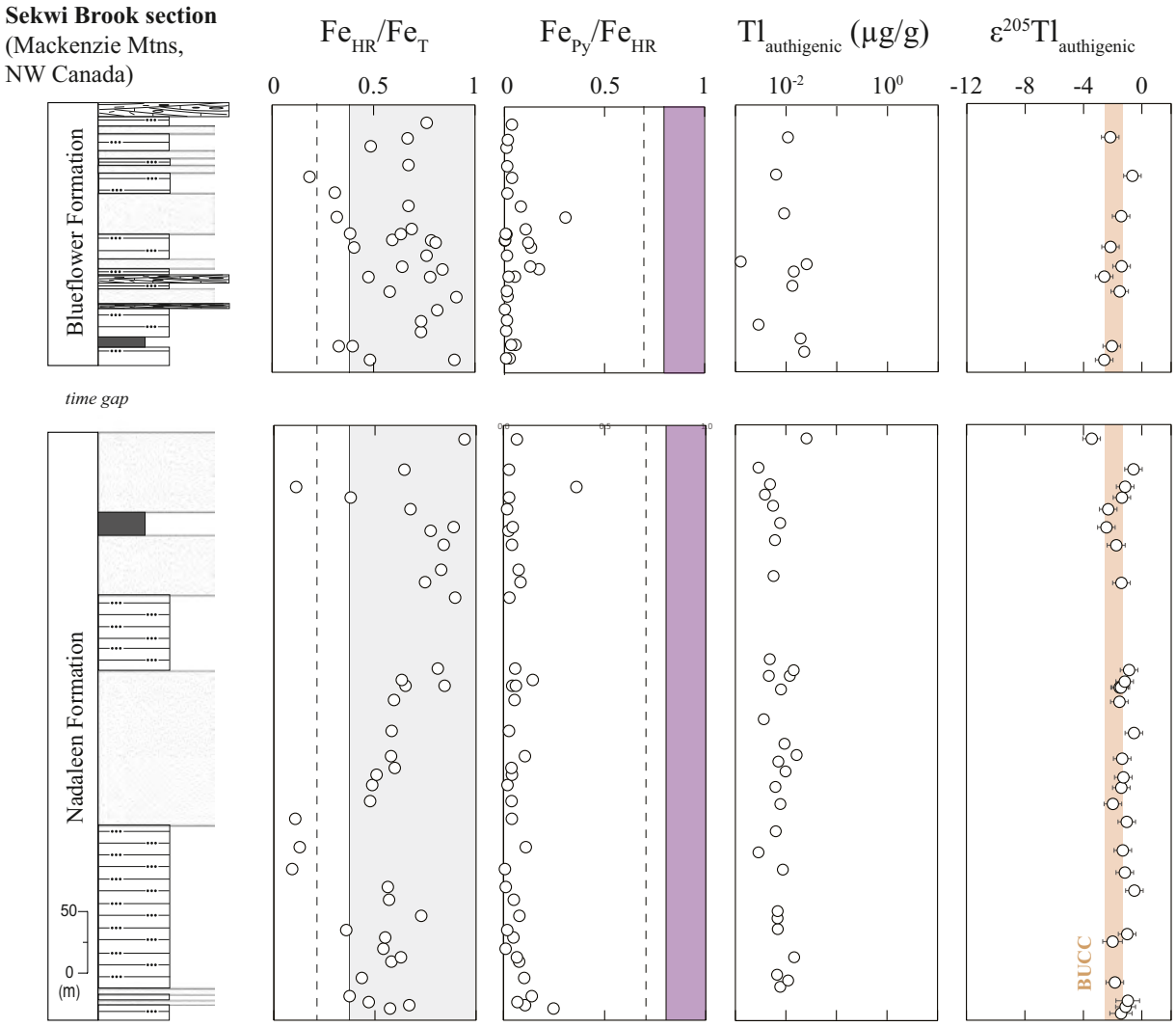


**Fig. 7.** Geochemistry of shales from the Sekwi Brook section. Stratigraphy is modified from Sperling et al. (2016) and Fe speciation data are from the same study. The grey and purple shaded areas signify the range of Fe speciation values indicative of anoxic ($Fe_{HR}/Fe_T \geq 0.38$) and euxinic ($Fe_{Py}/Fe_{HR} \geq 0.80$) local redox conditions, respectively (Poulton and Canfield, 2011). Dashed lines signify relaxed thresholds ($Fe_{HR}/Fe_T \geq 0.22$ and $Fe_{Py}/Fe_{HR} \geq 0.70$ (Poulton and Canfield, 2011)). White circles signify shale samples deposited under non-euxinic conditions (in this case, all samples). The brown shaded region in the Tl isotope plot signifies the range of values for the bulk upper continental crust ($\varepsilon^{205}Tl_{BUCC} = -2.1 \pm 0.3$ (Nielsen et al., 2005)). (For interpretation of the references to color in this figure legend, the reader is referred to the web version of this article.)

("IN") and the three principal outputs ("OUT", but more specifically "OXIC" = Mn oxide-rich sediments deposited beneath oxygenated bottom waters; "AOC" = low-T alteration of oceanic crust; and "ANOXIC" = sediments deposited beneath anoxic bottom waters), and $f_X$ is the respective output flux contribution (summarized also in Fig. 1). Because the differences between $\varepsilon^{205}Tl_{SW}$ and these outputs (that is, $\Delta_{OXIC}$, $\Delta_{AOC}$, and $\Delta_{ANOXIC}$; values summarized in Table 2) have been constrained experimentally and in modern marine settings, $\varepsilon^{205}Tl$ for each output can also be expressed as $\varepsilon^{205}Tl_{SW} - \Delta_{OUT}$:

$$\varepsilon^{205}Tl_{IN} = (\varepsilon^{205}Tl_{SW} - \Delta_{OXIC})(f_{OXIC}) + (\varepsilon^{205}Tl_{SW} - \Delta_{AOC})(f_{AOC}) + (\varepsilon^{205}Tl_{SW} - \Delta_{ANOXIC})(f_{ANOXIC}). \quad (2)$$

By performing these substitutions, ranges for $f_x$ can be calculated for any given $\varepsilon^{205}Tl_{SW}$ estimate. As a reference, open-ocean seawater today has a globally homogenous $\varepsilon^{205}Tl_{SW}$ of $-6.0 \pm 0.3$; 2SD (Nielsen et al., 2006; Owens et al., 2017). This $\varepsilon^{205}Tl$ value has been set primarily by Tl removal during oceanic crust alteration ($f_{AOC} = 0.64$) and by Tl delivery to marine sediments deposited beneath oxygenated bottom waters ($f_{OXIC} = 0.32$), and to a much lesser extent by Tl delivery to marine sediments deposited under anoxic bottom waters ($f_{ANOXIC} = 0.04$) ($f_X$ are calculated from Nielsen et al., 2017 and Owens et al., 2017; see Fig. 8 for a graphical illustration).

If the extremely negative $\varepsilon^{205}Tl_{authigenic}$ from the Doushantuo Formation do fingerprint globally homogenous Ediacaran open ocean $\varepsilon^{205}Tl$ values, they imply that $f_{OXIC}$ was an even more prominent marine

**Table 2**
Tl isotope mass-balance parameters used in Eq. (2).

| | $\varepsilon^{205}Tl$ | $\Delta_{OUT}$ | Ref. |
|---|---|---|---|
| Inputs | −1.8 | | 1 |
| Outputs | | | |
| OXIC | +10 | −16 | 1 |
| AOC | −7.4[a] | +1.4 | |
| ANOXIC | −6 | 0 | 2, 3 |

References: 1. Nielsen et al. (2017); 2. Owens et al. (2017); 3. Fan et al. (2020).
[a] This value is adjusted slightly from Ref. 1 to achieve mass-balance. Ref. 1 did not include anoxic sediments as a principal output. We have added this anoxic output and estimate its $f$ and $\Delta$ based on Ref. 2 (see their Fig. 1).

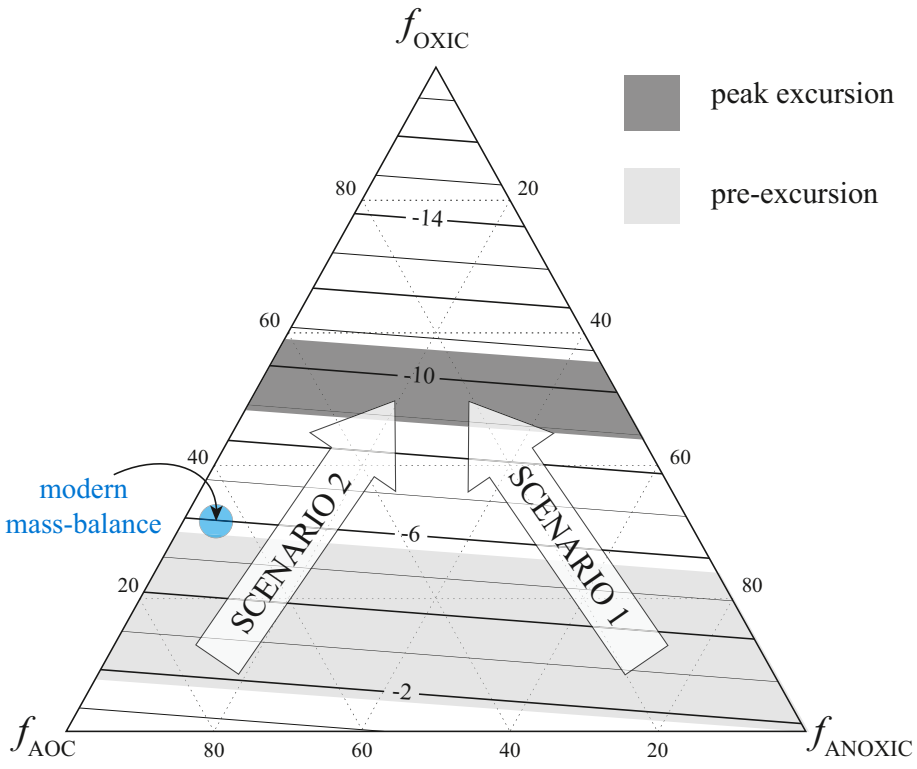


**Fig. 8.** Results of our Tl isotope mass-balance calculations plotted in a ternary diagram. Lines inside the diagram represent the open ocean $\varepsilon^{205}Tl_{SW}$ that results from the combination of $f_{OXIC}$, $f_{AOC}$, and $f_{ANOXIC}$ at that point in the diagram. Modern Tl isotope mass-balance, and the resultant $\varepsilon^{205}Tl_{SW}$, is plotted in blue for reference. Our most negative $\varepsilon^{205}Tl_{authigenic}$ from the Doushantuo formation are plotted in dark grey, while those values immediately preceding the excursions are plotted in light grey. The white arrows signify theoretical scenarios that could drive the negative Tl isotope excursions found in the Doushantuo Formation. See Section 5.1.1. for more details and also for acronym definitions. (For interpretation of the references to color in this figure legend, the reader is referred to the web version of this article.)

sink for Tl at these times than in the modern ocean (illustrated in Fig. 8). There are large ranges of $f_{AOC}$ and $f_{ANOXIC}$ values that can explain these negative $\varepsilon^{205}Tl_{SW}$ estimates, but all scenarios require a substantial $f_{OXIC}$ contribution ($f_{OXIC} \geq 0.44$). Put another way, $f_{OXIC}$ would have needed to increase substantially at these times during the Ediacaran at the expense of $f_{AOC}$ and/or $f_{ANOXIC}$.

We argue that one simplified scenario—an increase in $f_{OXIC}$ primarily at the expense of $f_{ANOXIC}$ ("Scenario 1" in Fig. 8)—is unlikely. In its most simple form, this scenario implies global Ediacaran oceans became better oxygenated during both negative $\varepsilon^{205}Tl_{authigenic}$ excursions than during the intervals outside of them. First and foremost, the negative $\varepsilon^{205}Tl_{authigenic}$ excursions occur outside of the purported OOEs, and if interpreted in this manner are therefore a direct contradiction of the OOE hypothesis (Sahoo et al., 2016). Some studies do infer enhanced ocean oxygenation outside of the OOEs, most often concurrent with or even as the driving force of the Shuram CIE (e.g., Fike et al., 2006; McFadden et al., 2008; Zhang et al., 2019, but also see Knauth and Kennedy, 2009; and Derry, 2010 for alternative hypotheses). Because the younger of our two negative $\varepsilon^{205}Tl_{authigenic}$ excursions occurs in the same Doushantuo Member that hosts the Shuram Excursion (Member III (Jiang et al., 2011)), this Tl isotope excursion could add credence to the ocean oxygenation hypothesis (the preferred interpretation of Fan et al., 2020). The older and greater magnitude negative $\varepsilon^{205}Tl_{authigenic}$ excursion revealed here (that is, the one observed in mid-Member II), however, does not align in time with any supporting evidence for enhanced global ocean oxygenation. An absence of corroborating evidence for widespread ocean oxygenation during deposition of mid-Member II does not eliminate the possibility, but it does not at the moment provide strong support for this simple explanation for both negative $\varepsilon^{205}Tl_{authigenic}$ excursions.

The alternate simplified scenario—an increase in $f_{OXIC}$ primarily at the expense of $f_{AOC}$ ("Scenario 2" in Fig. 8)—is also doubtful. A reduction in $f_{AOC}$ would imply that at these times during the Ediacaran low-T hydrothermal circulation worldwide was perturbed so that Tl removal into this output diminished. As an example, it is possible that at times in Earth's past when global sedimentation rates increased (e.g., as a result of enhanced terrestrial weathering), thick blankets of sediment could have prevented the percolation of fluids into some off-axis basalts, with those closest to the ocean margins likely receiving this weathered material. Alternatively, sluggish oceanic crust production rates at times in Earth's past could have reduced the areal extent of seafloor undergoing low-T alteration. Both of these scenarios are admittedly highly simplified and do not take into consideration much of the complexity associated with hydrothermal circulation in ocean crust (for example, see Mottl, 2003). Notwithstanding, either of these scenarios or any others that would have at times reduced the relative flux of Tl into altered oceanic crust would have diminished removal of the lighter-mass Tl isotope from seawater, in-turn facilitating its accumulation in seawater. It is worth noting that such scenarios would be expected to unfold over fairly long timescales. This possibility agrees with the progressive nature of the negative $\varepsilon^{205}Tl_{authigenic}$ excursions, which occur over 10s of millions-of-years according to the age estimates of Sahoo et al. (2016). It is additionally worth noting that an increase in seawater $\delta^{238}U$ was recently inferred across the Ediacaran Shuram CIE (Zhang et al., 2019), roughly coincident with the extremely negative $\varepsilon^{205}Tl_{authigenic}$ found here in upper-Member III and recently in another study (Fan et al., 2020). A global increase in seawater $\delta^{238}U$ would also be an expected consequence of diminished low-T hydrothermal circulation because of the predicted decrease in preferential removal of heavier-mass U isotopes from seawater into this U output (Andersen et al., 2015). Still, despite some of the merits of this hypothesis, we would argue that caution is warranted pending additional independent evidence for a dramatic change to global low-T ocean crust alteration processes during the Ediacaran.

### 5.1.2. *Plausible links to local-scale processes*

A more plausible explanation for the negative $\varepsilon^{205}Tl_{authigenic}$ excursions in the Doushantuo Formation is local controls. This hypothesis gains support, first and foremost, from the many independent lines of evidence that point to deposition of this formation in a semi-restricted basin concurrent with both $\varepsilon^{205}Tl_{authigenic}$ excursions (that is, between the purported OOEs at the Wuhe site; see Fig. 4 (Ostrander et al.,

2019a)). By analogy with modern restricted settings (e.g., the Black Sea (Owens et al., 2017)), it is possible that $\varepsilon^{205}Tl_{SW}$ in the basin at these times was strictly a local signature, independent of the open ocean $\varepsilon^{205}Tl_{SW}$. If so, then this local $\varepsilon^{205}Tl_{SW}$ would have been set exclusively by Tl mass-balance in the local basin.

There are basin-scale controls that could drive a local $\varepsilon^{205}Tl_{SW}$ signature to be very negative. For example, although local-scale heterogeneity in $\varepsilon^{205}Tl$ values of oceanic inputs is, from a mass-balance perspective, not likely to drive large variations in open-ocean $\varepsilon^{205}Tl_{SW}$ (Baker et al., 2009), heterogeneity could affect $\varepsilon^{205}Tl$ of the waters in a restricted basin. River water in some locations today has a considerably lighter $\varepsilon^{205}Tl$ relative to bulk continental crust (as low as $\varepsilon^{205}Tl = -6.8 \pm 1.5$ in the Danube (Nielsen et al., 2005)), as do some volcanic emissions (as low as $-16.7 \pm 0.5$ in Kilauea, HI (Baker et al., 2009)). If the principal Tl source(s) to the local Nanhua Basin approached or exceeded these modern $\varepsilon^{205}Tl$ values, mass-balance in the basin could have been skewed in that same direction – especially if this basin received little to no additional Tl from the open ocean.

A case could also be made that outputs of Tl in a restricted basin, namely Mn oxide-bearing sediments, would be very efficient in driving a negative $\varepsilon^{205}Tl$ in surface waters. First, a basin that exchanges little to no Tl with the open ocean would be minimally affected, if at all, by altered oceanic crust. In other words, a basin where very little or no seawater is circulated through oceanic crust, Tl isotope mass-balance in the basin would be controlled only by the relative distribution of oxic versus anoxic sediments in that basin. Going one step further, because Mn oxide-bearing oxic sediments would be the only Tl output that imparts an isotope fractionation effect in this scenario, and in fact a substantial effect (Rehkämper et al., 2002; Nielsen et al., 2013), isotope mass-balance in the basin would be strongly controlled by Mn oxides. This Mn oxide control, by preferentially removing the heavier-mass Tl isotope, would drive a lighter $\varepsilon^{205}Tl$ in surface waters.

Importantly, local operation of a Mn oxide "shuttle" in the Nanhua Basin during the purported OOEs, as is suggested by extremely negative $\delta^{98}Mo$ in the same samples (Ostrander et al., 2019a), cannot explain the shifts to more positive $\varepsilon^{205}Tl_{authigenic}$ values at these times. In theory, isotopically heavy Tl bound to Mn oxide minerals formed in oxygenated surface waters could be 'shuttled' to underlying anoxic marine sediments. Notably, however, our heavier $\varepsilon^{205}Tl_{authigenic}$ values are not limited to the OOE intervals (Fig. 4). Second, if the shuttle were operating, we would predict a substantial increase in Tl/Mo ratios and $\varepsilon^{205}Tl_{authigenic}$ during the OOEs (illustrated in Fig. 9). This prediction lies with the observation that Tl/Mo ratios in Mn oxide-replete ferromanganese crusts and nodules today (Tl/Mo = ~0.3 (Hein and Koschinsky, 2014)) are two orders of magnitude greater than those found in anoxic marine sediments from Cariaco Basin (Tl/Mo = ~0.007; calculated from Tl data reported in Owens et al., 2017 and Mo data summarized in Algeo and Lyons, 2006). Additionally, $\varepsilon^{205}Tl$ in ferromanganese crusts and nodules today ($\varepsilon^{205}Tl = \sim +10$ (Rehkämper et al., 2002; Nielsen et al., 2013)) are substantially heavier than those found in sediments from Cariaco Basin ($\varepsilon^{205}Tl = -5.1 \pm 1.3$; 2SD (Owens et al., 2017)). These Mn oxide fingerprints are not found in shales deposited during the OOEs (Fig. 9). To the contrary, our heaviest $\varepsilon^{205}Tl_{authigenic}$ are accompanied by the lowest Tl/Mo ratios (in shales from OOE C). These findings suggest that a Mn oxide shuttle had little to no effect on our measured $\varepsilon^{205}Tl_{authigenic}$ during the purported OOEs.

### 5.2. Invariant Northwest Canada shale $\varepsilon^{205}Tl$ record

Our comparatively invariant northwest Canada shale $\varepsilon^{205}Tl$ record supports the idea of local-scale processes driving much of the $\varepsilon^{205}Tl$ variability in South China shales. First, shales from the Nadaleen Formation (Sekwi Brook), which are inferred to be roughly coeval with pre-Shuram CIE Doushantuo Member III (Macdonald et al., 2013; Moynihan et al., 2019; see also Fig. 2), do not possess any extremely negative $\varepsilon^{205}Tl_{authigenic}$ values (Fig. 7). Instead, $\varepsilon^{205}Tl_{authigenic}$ in the Nadaleen are fairly invariant and near-crustal ($\varepsilon^{205}Tl_{authigenic} = -1.4 \pm 1.2$; 2SD). Shales from the Nadaleen are thought to have been deposited under predominantly ferruginous conditions (Sperling et al., 2016). No investigations have been conducted on Tl isotope cycling in modern ferruginous settings, but a recent study did investigate Tl isotopes in sediments deposited beneath modern anoxic and $H_2S$-poor waters (Santa Barbara Basin (Fan et al., 2020)). The authors showed that anoxic core-top sediments from the Santa Barbara Basin possessed $\varepsilon^{205}Tl_{authigenic}$ indistinguishable from globally homogenous $\varepsilon^{205}Tl_{SW}$ ($\varepsilon^{205}Tl_{authigenic} = -5.6 \pm 0.2$; 2SD (Fan et al., 2020) compared to $\varepsilon^{205}Tl_{SW} = -6.0 \pm 0.3$; 2SD (Nielsen et al., 2006; Owens et al., 2017)). Though the analogy between the modern Santa Barbara Basin and an ancient ferruginous setting is not perfect, it is possible that shales from the Nadaleen Formation also captured overlying $\varepsilon^{205}Tl_{SW}$ at the time of their deposition. Regardless of the absolute relevance of the analogy, and despite the difficulties associated with precisely correlating the Nadaleen with pre-Shuram CIE Doushantuo Member III at Wuhe (because of the difficulty locating the Shuram CIE at the latter site; see Section 2.3), the observation that shales from the Nadaleen exhibit invariant $\varepsilon^{205}Tl$ is compelling evidence against dramatic perturbation to global $\varepsilon^{205}Tl_{SW}$ across this timeframe.

Additionally, and perhaps more substantially, there is broad agreement between both shale records when they are inferred to have been deposited simultaneously (or nearly so) under the ideal conditions for capture of a globally homogenous $\varepsilon^{205}Tl_{SW}$ (Fig. 10) – that is, under anoxic conditions in an open-ocean setting (like the Cariaco Basin (Owens et al., 2017) and Santa Barbara Basin (Fan et al., 2020) basins). These ideal conditions were first met in both locations during OOE A (~635 Ma), at the time of deposition for the lowermost Doushantuo Member II and the Sheepbed Formation. $\varepsilon^{205}Tl_{authigenic}$ in both of these shale records span a relatively muted range, primarily sitting around the bulk upper continental crust value ($\varepsilon^{205}Tl_{BUCC} = -2.1 \pm 0.3$ (Nielsen et al., 2005)) but also with a few noticeably lighter values (as low as $\varepsilon^{205}Tl_{authigenic} = -4.2 \pm 0.2$; 2SD in Member II and $-4.4 \pm 0.2$; 2SD in the Sheepbed Formation). Conditions ideal for capture of a globally homogenous $\varepsilon^{205}Tl_{SW}$ were also met in both locations in the broader timeframe following the Shuram CIE, during deposition of Doushantuo Member IV and the Blueflower Formation

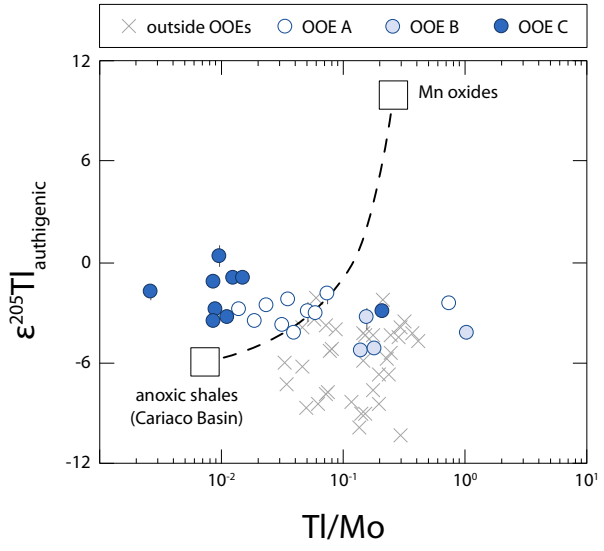


**Fig. 9.** Semi-log plot of our $\varepsilon^{205}Tl_{authigenic}$ and Tl/Mo ratios from Doushantuo shales. The dashed line signifies modern mixing between an anoxic shale component from the Cariaco Basin and Mn oxide minerals (see text for references). If Tl had been at times delivered to the shales of the Doushantuo Formation by Mn oxide minerals, this is the mixing trend we would predict.

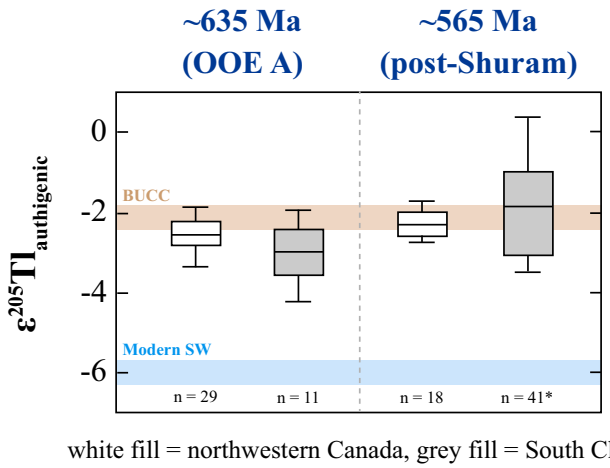


**Fig. 10.** Box and whisker plots of Tl isotope data from some roughly time contemporaneous Ediacaran shales in our study. The $\varepsilon^{205}$Tl of bulk upper continental crust (BUCC) comes from Nielsen et al. (2005), and for modern seawater comes from Nielsen et al. (2006) and Owens et al. (2017). All data from northwestern Canada shales is from this study. Data from all ~635 Ma South China shales is from this study, while some data from post-Shuram CIE shales comes from Fan et al. (2020) (annotated by the asterisk).

(~565 Ma (Rooney et al., 2020)). Likewise, $\varepsilon^{205}Tl_{authigenic}$ from these shale intervals are overwhelmingly near-crustal and only at times slightly lighter than crust (as low as $\varepsilon^{205}Tl_{authigenic} = -3.5 \pm 0.2$; 2SD in Member IV and $-2.7 \pm 0.2$; 2SD in the Blueflower Formation at Goz A). Across this second timeframe, predominantly near-crustal $\varepsilon^{205}Tl_{authigenic}$ were also recently found in Member IV equivalents from different sections in South China (i.e., EN3c (Fan et al., 2020)). This broad agreement at ~635 Ma and ~565 Ma is, we argue, strong evidence that a globally homogenous $\varepsilon^{205}Tl_{SW}$ was captured in these sedimentary records at these times, or nearly so (latter point expanded upon below).

A few of our shale samples from northwestern Canada are thought to have been deposited under $O_2$-bearing bottom waters and as such may not have captured past $\varepsilon^{205}Tl_{SW}$. For example, in the Blueflower Formation at Sekwi Brook, the presence at times of bilaterian burrows likely represent evidence for intermittent oxygenation (Sperling et al., 2016). If the in-situ formation or burial of Mn oxides during this time affected our measured $\varepsilon^{205}Tl_{authigenic}$, we would predict heavier values (Rehkämper et al., 2002, 2004). Indeed, some of our measured $\varepsilon^{205}Tl_{authigenic}$ in shales from the Blueflower Formation at Sekwi Brook are slightly heavier than their equivalents from Goz A (as heavy as $\varepsilon^{205}Tl_{authigenic} = -0.7 \pm 0.6$; 2SD; Fig. 7), suggesting that local Mn oxide formation in this paleo-location may have skewed some sedimentary $\varepsilon^{205}$Tl. Notably, however, it is unlikely that the full positive Tl isotope fractionation effect between seawater and Mn oxides was imparted on the original Sekwi Brook sediments ($\Delta_{SW\text{-}OXIDE} = \sim -19$ (Rehkämper et al., 2002; Nielsen et al., 2013)). If this were the case, we would expect these sedimentary $\varepsilon^{205}Tl_{authigenic}$ to be substantially heavier than those from Goz A – not just slightly heavier. In the lower Sheepbed Formation at Goz A, a transient Mn enrichment is interpreted as evidence for the brief encroachment of oxic local surface waters (concurrent with a maximum flooding surface, or MFS (Johnston et al., 2013); see Fig. 6). In this case, local Mn oxide burial was likely absent, evidenced by no noticeable variation in our measured $\varepsilon^{205}Tl_{authigenic}$ across the MFS (Fig. 6). In sum, it is reasonable to assume that most of our northwestern Canada shales may have captured open ocean $\varepsilon^{205}Tl_{SW}$, or nearly so.

### 5.3. Ediacaran ocean oxygenation

The question remains whether connections can be made between our Tl isotope dataset and Ediacaran global ocean oxygenation. To this end, we focus on the time intervals during which we can most confidently track Ediacaran open ocean $\varepsilon^{205}Tl_{SW}$ (discussed in Section 5.2). To recap, these intervals include ~635 Ma (OOE A, during deposition of lowermost Doushantuo Member II and the Sheepbed Formation), ~580 Ma (OOE B, during deposition of lowermost Doushantuo Member III), ~575 Ma (pre-Shuram CIE, during deposition of the Nadaleen Formation), and ~565 Ma (post-Shuram CIE, during deposition of Doushantuo Member IV and the Blueflower Formation).

At times during the Ediacaran when our shale data imply a predominantly near-crustal $\varepsilon^{205}Tl_{SW}$ ($\varepsilon^{205}Tl_{BUCC} = -2.1 \pm 0.3$ (Nielsen et al., 2005)), the most straightforward interpretation is a global ocean with limited accumulation of $O_2$ in marine bottom waters. As discussed in the previous section, a predominantly near-crustal open ocean $\varepsilon^{205}Tl_{SW}$ can be inferred from most shales deposited at ~635 Ma, ~575 Ma, and ~565 Ma. In order to support such a heavy open ocean seawater Tl isotope signature at these times, the fraction of Tl removal from the ocean into Mn oxide-bearing marine sediments must have been very low (less than about ~15% of the global Tl removal flux, compared to 32% today; see Section 5.1.1 and Fig. 8). By inference, the conditions required to promote sedimentary Mn oxide burial – that is, accumulation of $O_2$ in marine bottom waters (Calvert and Pedersen, 1996) – must have also been quite rare. Because the overwhelming majority of our entire shale dataset imply a near-crustal $\varepsilon^{205}Tl_{SW}$, it seems reasonable to assume that $O_2$ did not commonly accumulate in marine bottom waters worldwide during the Ediacaran Period. In other words, the "baseline" ocean oxygenation state for the Ediacaran Period was probably one with limited $O_2$ accumulation in marine bottom waters.

For comparatively much briefer periods of time during the Ediacaran, when our shale data imply a considerably lighter-than-crustal open ocean $\varepsilon^{205}Tl_{SW}$, the most straightforward interpretation is a global ocean with transiently enhanced accumulation of $O_2$ in marine bottom waters. In brief, widespread accumulation of $O_2$ in bottom waters would be predicted to enhance Mn oxide burial in marine sediments worldwide, in-turn promoting the preferential accumulation of the lighter-mass Tl isotope in seawater (Owens et al., 2017). A transiently more negative $\varepsilon^{205}Tl_{SW}$ can be inferred from shales deposited around ~635 Ma (as low as $\varepsilon^{205}Tl_{SW} = -4.4 \pm 0.2$; 2SD during deposition of the Sheepbed Formation; Fig. 6), and also from shales deposited around ~580 Ma (as low as $\varepsilon^{205}Tl_{SW} = -5.3 \pm 0.3$; 2SD during deposition of lowermost Doushantuo Member III; Fig. 4). In both cases, the idea of a transiently better oxygenated global ocean is also supported by strong RSE enrichments in coeval shales from South China (that is, previously noted evidence for these OOEs (Sahoo et al., 2012, 2016)).

Notably, only a few shale samples deposited during the ~635 Ma OOE reveal a considerably lighter-than-crustal $\varepsilon^{205}Tl_{SW}$ (within lowermost Doushantuo Member II and the Sheepbed Formation; evident in Figs. 3 and 5), and no shale samples deposited around the time of the ~565 Ma OOE (again, see Rooney et al., 2020 for this revised age estimation for OOE-C) reveal such values (within Doushantuo Member IV and the Blueflower Formation; evident in Figs. 3, 5, and 6). The rare occurrence of a considerably negative $\varepsilon^{205}Tl_{SW}$ during these two OOEs suggests that widespread sedimentary Mn oxide burial was very rare during these events – in the case of the ~565 Ma, perhaps even non-existent. By extension, widespread accumulation of $O_2$ in marine bottom waters during these events was probably also rare, occurring over timescales much shorter than the purported < 5–10 myr durations of the OOEs (Sahoo et al., 2016).

If $O_2$ was not persistently widespread in marine bottom waters for the duration of the Ediacaran OOEs, why do RSE abundances reach such high levels in the Doushantuo Formation during these events? As was mentioned in the introduction, there are multiple local-scale controls that have almost certainly affected the sedimentary RSE enrichment patterns in shales from the Doushantuo Formation. These include

the development of a local particulate shuttle (Ostrander et al., 2019a) as well as the condensed nature of Ediacaran stratigraphic sections from South China (Miller et al., 2017). Alone or together, these local-scale controls probably played some role in accentuating sedimentary RSE enrichments, at least compared to those in shales deposited in northwestern Canada. In addition, it is to be expected that changes in marine bottom-water $O_2$ accumulation in particular would not affect every RSE reservoir in the same way. It is well-known that each of these RSEs is sensitive to different specific redox conditions (e.g., suboxic, anoxic, euxinic, etc.; discussed in detail in Tribovillard et al., 2006 and Bennett and Canfield, 2020). As an example, it is possible that, at times during the Ediacaran Period, global ocean oxygenation levels were higher than those typically present during the Neoproterozoic but not high enough to allow for such strong and widespread accumulation of $O_2$ in global bottom waters and sediments as was found during the younger Phanerozoic Eon. In this hypothetical scenario, many marine sediments may have been only weakly oxygenated (e.g., deposited under suboxic conditions), preventing the efficient removal of many RSEs from seawater while at the same time also preventing the formation and burial of Mn oxide minerals (e.g., Morford et al., 2005). Such a scenario could be predicted to enhance the size of global seawater RSE reservoirs, but not promote widespread burial of Mn oxide minerals in marine sediments – similar to what can be inferred from shales deposited during these events. In other words, these Ediacaran OOEs may represent an intermediate Proterozoic-Phanerozoic global ocean oxygenation state.

If widespread and pervasive ocean oxygenation on par with that observed today did occur during the rise of complex life, it probably occurred only for relatively brief periods of time. For example, the initial appearance of the first assemblage of the Ediacaran Biota (i.e., the Avalon assemblage, ~574 Ma) seems to have taken place in a predominantly low-$O_2$ world (Rooney et al., 2020). Our new Tl isotope data also support this notion because shales from the Nadaleen Formation host (a) fossils from the Avalon assemblage (Narbonne et al., 2014), (b) iron speciation evidence for locally reducing conditions (Sperling et al., 2016), and (c) $\varepsilon^{205}$Tl indicative of limited global Mn oxide burial. It is not until after the initial appearance of the Avalon assemblage, during the Shuram CIE, that global ocean oxygenation levels perhaps approached near-modern levels (according to U isotope ratios in carbonates (Zhang et al., 2019)). After the Shuram CIE, and on the eve of the rise of the White Sea assemblage (~560 Ma to ~550 Ma (Boag et al., 2016)), our Tl isotope data suggest that global ocean oxygenation levels once again returned to lower-than-modern levels (but see Kendall et al., 2015). The Nama assemblage (~550 Ma to ~541 Ma (Boag et al., 2016)) also seems to have inhabited a predominantly anoxic global ocean (e.g., Zhang et al., 2018). In sum, the Ediacaran Biota seems to have flourished, overwhelmingly, in a global ocean that was not as strongly oxygenated as today (Sperling et al., 2015a, 2015b).

## 6. Conclusions

Careful attempts at reconstructing Earth's past environments demand multiple approaches considered in the full geochemical, oceanographic, and geological context. Shales from South China reveal two extremely negative $\varepsilon^{205}Tl_{authigenic}$ excursions, while $\varepsilon^{205}Tl_{authigenic}$ in their coeval equivalents from northwestern Canada are generally invariant. Much of this geochemical disparity can be reconciled by invoking local-scale differences between the individual paleo-depositional sites. The most critical difference would have been the degree of open-ocean connection at each site and how this connectivity changed during the Ediacaran Period.

We find much better agreement in our Tl isotope records if we look exclusively at shales deposited in settings likely to have been well connected to the open ocean. Today's globally homogenous $\varepsilon^{205}Tl_{SW}$ is captured in marine sediments only when deposited in basins that maintain a strong connection to the open ocean (e.g., the Cariaco (Owens et al., 2017) and Santa Barbara (Fan et al., 2020) basins). The most pronounced negative $\varepsilon^{205}Tl_{authigenic}$ excursions in South China are found in shales possibly deposited under restricted conditions. In modern restricted basins (e.g., the Black Sea (Owens et al., 2017)), Tl isotope mass-balance is regulated exclusively by local controls (e.g., $\varepsilon^{205}$Tl of local inputs and Mn oxide burial within the basin).

When we are able to reconstruct Ediacaran open ocean $\varepsilon^{205}Tl_{SW}$, we find that this value was predominantly comparable to or only slightly lighter than that of the bulk upper continental crust ($\varepsilon^{205}Tl_{BUCC} = -2.1 \pm 0.3$ (Nielsen et al., 2005)). Such a persistent and heavy open ocean $\varepsilon^{205}Tl_{SW}$ implies limited Mn oxide burial in global marine sediments for large periods of time during the Ediacaran and by inference also limited accumulation of $O_2$ in global marine bottom waters. Only for very brief periods (≪5–10 million years) during the Ediacaran Period at ~635 Ma and ~580 Ma does open ocean $\varepsilon^{205}Tl_{SW}$ seem to have reached values considerably lighter than bulk upper continental crust (for example, $\varepsilon^{205}Tl_{SW}$ as low as $-4.4 \pm 0.2$; 2SD at ~635 Ma and $-5.3 \pm 0.3$; 2SD at ~580 Ma). These transiently more negative $\varepsilon^{205}Tl_{SW}$ fingerprint very brief episodes of widespread sedimentary Mn oxide burial and by inference very brief episodes of widespread accumulation of $O_2$ in marine bottom waters during the evolution of animals in the Ediacaran.

One logical next step would be to constrain open ocean $\varepsilon^{205}Tl_{SW}$ using additional Ediacaran shale records. There are some timeframes during the Ediacaran Period for which our inferences of past $\varepsilon^{205}Tl_{SW}$ are based solely on one set of shales (e.g., the ~580 Ma OOE preserved in shales only from South China), and some timeframes during which we are unable to confidently estimate $\varepsilon^{205}Tl_{SW}$ whatsoever (e.g., most of the timeframe separating the ~635 Ma and ~580 Ma OOEs). Regarding the ~580 Ma OOE, it would also be beneficial to provide a more robust age estimate for this event seeing as it approaches the timeframe of the initial appearance of the Ediacaran Biota (~574 Ma (Rooney et al., 2020)). The strata that hosts this OOE is particularly hard to correlate with age-equivalent sections, even those from the same area in South China (i.e., lowermost Doushantuo Member III (Jiang et al., 2011)). A more robust and complete Ediacaran $\varepsilon^{205}Tl_{SW}$ record, and by association also a more complete Ediacaran deep-marine oxygenation record, could be constructed simply by targeting additional sets of shales for Tl isotope analyses. It would be ideal for these prospective studies to target shales from multiple locations that were deposited under local anoxic conditions. Some possible targets are early- to mid-Ediacaran shales from South Australia and East Greenland (Canfield et al., 2008) and mid- to late-Ediacaran shales from Newfoundland (Canfield et al., 2007), Uruguay (Frei et al., 2013), and the Czech Republic (Kurzweil et al., 2015). As our study shows, future efforts will require careful consideration of all processes and controls operating at each location to unmix local and global controls.

## Declaration of competing interest

The authors declare that they have no known competing financial interests or personal relationships that could have appeared to influence the work reported in this paper.

## Acknowledgments

We would like to thank Jurek Blusztajn for his help with instrumental analysis at Woods Hole Oceanographic Institution. We would also like to thank Huan Cui and another anonymous reviewer for providing constructive comments on the manuscript. This research was supported financially by NSF grant OCE 1434785 (to J.D.O. and S.G.N.), NASA Exobiology grants NNX16AJ60G (to J.D.O. and S.G.N.) and 80NSSC18K1532 (J.D.O.), and the NASA Astrobiology Institute under Cooperative Agreement No. NNA15BB03A issued through the Science Mission Directorate also provided funds (T.W.L.). A portion of

this work was performed at the National High Magnetic Field Laboratory (Tallahassee, Florida), which is supported by the National Science Foundation Cooperative Agreement No. DMR-1644779 and the State of Florida. This material is based upon work supported by the National Science Foundation Graduate Research Fellowship Program under Grant No. 026257-001 (C.M.O.). Any opinions, findings, and conclusions or recommendations expressed in this material are those of the authors and do not necessarily reflect the views of the National Science Foundation.

## Appendix A. Supplementary data

Supplementary data to this article can be found online at https://doi.org/10.1016/j.chemgeo.2020.119856.

## References

Algeo, T.J., Lyons, T.W., 2006. Mo-total organic carbon covariation in modern anoxic marine environments: implications for analysis of paleoredox and paleohydrographic conditions. Paleoceanography 21 (PA1016), 1–23.
An, Z., Jiang, G., Tong, J., Tian, L., Ye, Q., Song, H., Song, H., 2015. Stratigraphic position of the Ediacaran Miaohe biota and its constrains on the age of the upper Doushantuo $\delta^{13}C$ anomaly in the Yangtze Gorges area, South China. Precambrian Res. 271, 243–253.
Andersen, M.B., Elliott, T., Freymuth, H., Sims, K.W.W., Niu, Y., Kelley, K.A., 2015. The terrestrial uranium isotope cycle. Nature 517, 356–359.
Baker, R.G.A., Rehkämper, M., Hinkley, T.K., Nielsen, S.G., Toutain, J.P., 2009. Investigation of thallium fluxes from subaerial volcanism—implications for the present and past mass balance of thallium in the ocean. Geochim. Cosmochim. Acta 73, 6340–6359.
Bennett, W.W., Canfield, D.E., 2020. Redox-sensitive trace metals as paleoredox proxies: a review and analysis of data from modern sediments. Earth Sci. Rev. 204, 103175.
Boag, T.H., Darroch, S.A.F., Laflamme, M., 2016. Ediacaran distributions in space and time: testing assemblage concepts of earliest macroscopic body fossils. Paleobiology 42, 574–594.
Bowman, C.N., Young, S.A., Kaljo, D., Eriksson, M.E., Them II, T.R., Hints, O., Martma, T., Owens, J.D., 2019. Linking the progressive expansion of reducing conditions to a stepwise mass extinction event in the late Silurian oceans. Geology 47, 968–972.
Calvert, S.E., Pedersen, T.F., 1996. Sedimentary geochemistry of manganese: implications for the environment of formation of manganiferous black shales. Econ. Geol. 91, 36–47.
Canfield, D.E., Poulton, S.W., Narbonne, G.M., 2007. Late-Neoproterozoic deep-ocean oxygenation and the rise of animal life. Science 315, 92–95.
Canfield, D.E., Poulton, S.W., Knoll, A.H., Narbonne, G.M., Ross, G., Goldberg, T., Strauss, H., 2008. Ferruginous conditions dominated later Neoproterozoic deep-water chemistry. Science 321, 949–952.
Cole, D.B., Mills, D.H., Erwin, D.B., Sperling, E.A., Porter, S.M., Reinhard, C.T., Planavsky, N.J., 2020. On the co-evolution of surface oxygen levels and animals. Geobiology 18, 260–281.
Condon, D., Zhu, M., Bowring, S., Wang, W., Yang, A., Jin, Y., 2005. U-Pb ages from the Neoproterozoic Doushantuo Formation, China. Science 308, 95–98.
Dalrymple, R.W., Narbonne, G.M., 1996. Continental slope sedimentation in the Sheepbed Formation (Neoproterozoic Windermere Supergroup), Mackenzie Mountains, N.W.T. Can. J. Earth Sci. 33, 848–862.
Derry, L.A., 2010. A burial diagenesis origin for the Ediacaran Shuram-Wonoka carbon isotope anomaly. Earth Planet. Sci. Lett. 294, 152–162.
Fan, H., Nielsen, S.G., Owens, J.D., Auro, M., Shu, Y., Hardisty, D.S., Horner, T.J., Bowman, C.N., Young, S.A., Wen, H., 2020. Constraining oceanic oxygenation during the Shuram excursion in South China using thallium isotopes. Geobiology 18, 348–365.
Fike, D.A., Grotzinger, J.P., Pratt, L.M., Summons, R.E., 2006. Oxidation of the Ediacaran ocean. Nature 444, 744–747.
Frei, R., Gaucher, C., Stolper, D., Canfield, D.E., 2013. Fluctuations in late Neoproterozoic atmospheric oxidation – Cr isotope chemostratigraphy and iron speciation of the late Ediacaran lower Arroyo del Soldado Group (Uruguay). Gondwana Res. 23, 797–811.
Gregory, D.D., Lyons, T.W., Large, R.R., Jiang, G., Stepanov, A.S., Diamond, C.W., Figueroa, M.C., Olin, P., 2017. Whole rock and discrete pyrite geochemistry as complementary tracers of ancient ocean chemistry: an example from the Neoproterozoic Doushantuo Formation, China. Geochim. Cosmochim. Acta 216, 201–220.
Hein, J., Koschinsky, A., 2014. Deep-ocean ferromanganese nodules and crusts. In: Scott, S. (Ed.), Treatise on Geochemistry 2nd Edition (TGC2), New Volume on Geochemistry of Mineral Deposits, 2nd ed. pp. 273–291.
Jiang, G., Kaufman, A.J., Christie-Blick, N., Zhang, S., Wu, H., 2007. Carbon isotope variability across the Ediacaran Yangtze platform in South China: implications for a large surface-to-deep ocean $\delta^{13}C$ gradient. Earth Planet. Sci. Lett. 261, 303–320.
Jiang, G., Shi, X., Zhang, S., Wang, Y., Xiao, S., 2011. Stratigraphy and paleogeography of the Ediacaran Doushantuo Formation (ca. 635–551 Ma) in South China. Gondwana Res. 19, 831–849.
Johnston, D.T., Poulton, S.W., Tosca, N.J., O'Brien, T., Halverson, G.P., Schrag, D.P., Macdonald, F.A., 2013. Searching for an oxygenation event in the fossiliferous Ediacaran of northwestern Canada. Chem. Geol. 362, 273–286.
Kendall, B., Komiya, T., Lyons, T.W., Bates, S.M., Gordon, G.W., Romaniello, S.J., Jiang, G., Creaser, R.A., Xiao, S., McFadden, K., Sawaki, Y., Tahata, M., Shu, D., Han, J., Li, Y., Chu, X., Anbar, A.D., 2015. Uranium and molybdenum isotope evidence for an episode of widespread ocean oxygenation during the late Ediacaran Period. Geochim. Cosmochim. Acta 156, 173–193.
Knauth, P., Kennedy, M.J., 2009. The late Precambrian greening of the Earth. Nature 460, 728–732.
Kurzweil, F., Drost, K., Pašava, J., Wille, M., Taubald, H., Schoeckle, D., Schoenberg, R., 2015. Coupled sulfur, iron, and molybdenum isotope data from black shales of the Teplá-Barrandian unit argue against deep ocean oxygenation during the Ediacaran. Geochim. Cosmochim. Acta 171, 121–142.
Li, C., Love, G.D., Lyons, T.W., Fike, D.A., Sessions, A.L., Chu, D., 2010. A stratified redox model for the Ediacaran ocean. Science 328, 80–83.
Li, X.Z., Evans, D.A.D., Halverson, G.P., 2013. Neoproterozoic glaciations in a revised global palaeogeography from the breakup of Rodinia to the assembly of Gondwanaland. Sediment. Geol. 294, 219–232.
Macdonald, F.A., Strauss, J.V., Sperling, E.A., Halverson, G.P., Narbonne, G.M., Johnston, D.T., Kunzmann, M., Schrag, D.P., Higgins, J.A., 2013. The stratigraphic relationship between the Shuram carbon isotope excursion, the oxygenation of Neoproterozoic oceans, and the first appearance of the Ediacaran biota and bilaterian trace fossils in northwestern Canada. Chem. Geol. 362, 250–272.
McFadden, K.A., Huang, J., Chu, X., Jiang, G., Kaufman, A.J., Zhou, C., Yuan, X., Xiao, S., 2008. Pulsed oxidation and biological evolution in the Ediacaran Doushantuo Formation. Proc. Natl. Acad. Sci. 105, 3197–3202.
Miller, A.J., Strauss, J.V., Halverson, G.P., Macdonald, F.A., Johnston, D.T., Sperling, E.A., 2017. Tracking the onset of Phanerozoic-style redox-sensitive trace metal enrichments: new results from basal Ediacaran post-glacial strata in NW Canada. Chem. Geol. 457, 24–37.
Morford, J.L., Emerson, S.R., Breckel, E.J., Kim, S.H., 2005. Diagenesis of oxyanions (V, U, Re, and Mo) in pore waters and sediments from a continental margin. Geochim. Cosmochim. Acta 69, 5021–5032.
Mottl, M.J., 2003. Partitioning of energy and mass fluxes between mid-ocean ridge axes and flanks at high and low temperature. In: Halbach, P. (Ed.), Energy and Mass Transfer in Marine Hydrothermal Systems. Dahlem University Press, Berlin, Germany, pp. 271–286.
Moynihan, D.P., Strauss, J.V., Nelson, L.L., Padget, C.D., 2019. Upper Windermere Supergroup and the transition from rifting to continent-margin sedimentation, Nadaleen River area, northern Canadian Cordillera. Geol. Soc. Am. Bull. 131, 1673–1701.
Narbonne, G.M., Laflamme, M., Trusler, P.W., Dairymple, R.W., Greentree, C., 2014. Deep-water Ediacaran fossils from northwestern Canada: taphonomy, ecology, and evolution. J. Paleontol. 88, 207–223.
Nielsen, S.G., Rehkämper, M., Baker, J.A., Halliday, A.N., 2004. The precise and accurate determination of thallium isotope compositions and concentrations for water samples by MC-ICPMS. Chem. Geol. 204, 109–124.
Nielsen, S.G., Rehkämper, M., Porcelli, D., Andersson, P., Halliday, A.N., Swarzenski, P.W., Latkoczy, C., Günther, D., 2005. Thallium isotopic composition of the upper continental crust and rivers – an investigation of the continental sources of dissolved marine thallium. Geochim. Cosmochim. Acta 19, 2007–2019.
Nielsen, S.G., Rehkämper, M., Teagle, D.A.H., Butterfield, D.A., Alt, J.C., Halliday, A.N., 2006. Hydrothermal fluid fluxes calculated from the isotopic mass balance of thallium in the ocean crust. Earth Planet. Sci. Lett. 251, 120–133.
Nielsen, S.G., Goff, M., Hesselbo, S.P., Jenkyns, H.C., LaRowe, D.E., Lee, C.A., 2011. Thallium isotopes in early diagenetic pyrite – a paleoredox proxy? Geochim. Cosmochim. Acta 75, 6690–6704.
Nielsen, S.G., Wasylenki, L.E., Rehkämper, M., Peacock, C.L., Xue, Z., Moon, E.M., 2013. Towards an understanding of thallium isotope fractionation during adsorption to manganese oxides. Geochim. Cosmochim. Acta 117, 252–265.
Nielsen, S.G., Rehkämper, M., Prytulak, J., 2017. Investigation and application of thallium isotope fractionation. Rev. Mineral. Geochem. 82, 759–798.
Och, L.M., Cremonese, L., Shields-Zhou, G.A., Poulton, S.W., Struck, U., Ling, H., Li, D., Chen, X., Manning, C.A., Thirlwall, M., Strauss, H., Zhu, M., 2016. Paleoceanographic controls on spatial redox distribution over the Yangtze Platform during the Ediacaran-Cambrian transition. Sedimentology 63, 378–410.
Ostrander, C.M., Owens, J.D., Nielsen, S.G., 2017. Constraining the rate of oceanic deoxygenation leading up to a Cretaceous Oceanic Anoxic Event (OAE-2: ~94Ma). Sci. Adv. 3, e1701020.
Ostrander, C.M., Sahoo, S.K., Kendall, B., Jiang, G., Planavsky, N.J., Lyons, T.W., Nielsen, S.G., Owens, J.D., Gordon, G.W., Romaniello, S.J., Anbar, A.D., 2019a. Multiple negative molybdenum isotope excursions in the Doushantuo Formation (South China) fingerprint complex redox-related processes in the Ediacaran Nanhua Basin. Geochim. Cosmochim. Acta 261, 191–209.
Ostrander, C.M., Nielsen, S.G., Owens, J.D., Kendall, B., Gordon, G.W., Romaniello, S.J., Anbar, A.D., 2019b. Fully oxygenated water columns over continental shelves before the Great Oxidation Event. Nat. Geosci. 12, 186–191.
Owens, J.D., Nielsen, S.G., Horner, T.J., Ostrander, C.M., Peterson, L.C., 2017. Thallium-isotopic compositions of euxinic sediments as a proxy for global manganese-oxide burial. Geochim. Cosmochim. Acta 213, 291–307.
Partin, C.A., Bekker, A., Planavsky, N.J., Scott, C.T., Gill, B.C., Li, C., Podkovyrov, V., Maslov, A., Konhauser, K.O., Lalonde, S.V., Love, G.D., Poulton, S.W., Lyons, T.W., 2013. Large-scale fluctuations in Precambrian atmospheric and oceanic oxygen levels from the record of U in shales. Earth Planet. Sci. Lett. 369-370, 284–293.
Peacock, C.L., Moon, E.M., 2012. Oxidative scavenging of thallium by birnessite: explanation for thallium enrichment and stable isotope fractionation in marine

ferromanganese precipitates. Geochim. Cosmochim. Acta 84, 297–313.
Planavsky, N.J., McGoldrick, P., Scott, C.T., Li, C., Reinhard, C.T., Kelly, A.E., Chu, X., Bekker, A., Love, G.D., Lyons, T.W., 2011. Widespread iron-rich conditions in the mid-Proterozoic ocean. Nature 477, 448–451.
Poulton, S.W., Canfield, D.E., 2011. Ferruginous conditions: a dominant feature of the ocean through Earth's history. Elements 7, 107–112.
Rehkämper, M., Halliday, A.N., 1999. The precise measurement of Tl isotopic compositions by MC-ICPMS: applications to the analysis of geological materials and meteorites. Geochim. Cosmochim. Acta 63, 935–944.
Rehkämper, M., Frank, M., Hein, J.R., Porcelli, D., Halliday, A., Ingri, J., Liebetrau, V., 2002. Thallium isotope variations in seawater and hydrogenetic, diagenetic, and hydrothermal ferromanganese deposits. Earth Planet. Sci. Lett. 197, 65–81.
Rehkämper, M., Frank, M., Hein, J.R., Halliday, A., 2004. Cenozoic marine geochemistry of thallium deduced from isotopic studies of ferromanganese crusts and pelagic sediments. Earth Planet. Sci. Lett. 219, 77–91.
Reinhard, C.T., Planavsky, N.J., Robbins, L.J., Partin, C.A., Gill, B.C., Lalonde, S.V., Bekker, A., Konhauser, K.O., Lyons, T.W., 2013. Proterozoic ocean redox and biogeochemical stasis. Proc. Natl. Acad. Sci. 111, 5357–5362.
Rooney, A.D., Strauss, J.V., Brandon, A.D., Macdonald, F.A., 2015. A Cryogenian chronology: two long-lasting synchronous Neoproterozoic glaciations. Geology 43, 459–462.
Rooney, A.D., Cantine, M.D., Bergmann, K.D., Gómez-Pérez, I., Al Baloushi, B., Boag, T.H., Busch, J.F., Sperling, E.A., Strauss, J.V., 2020. Calibrating the co-evolution of Ediacaran life and environment. Proc. Natl. Acad. Sci. 117, 16824–16830.
Sahoo, S.K., Planavsky, N.J., Kendall, B., Wang, X., Shi, X., Scott, C., Anbar, A.D., Lyons, T.W., Jiang, G., 2012. Ocean oxygenation in the wake of the Marinoan glaciation. Nature 489, 546–549.
Sahoo, S.K., Planavsky, N.J., Jiang, G., Kendall, B., Owens, J.D., Wang, X., Shi, X., Anbar, A.D., Lyons, T.W., 2016. Oceanic oxygenation events in the anoxic Ediacaran ocean. Geobiology 14, 457–468.
Scott, C., Lyons, T.W., Bekker, A., Shen, Y., Poulton, S.W., Chu, X., Anbar, A.D., 2008. Tracing the stepwise oxygenation of the Proterozoic ocean. Nature 452, 456–459.
Sheen, A.I., Kendall, B., Reinhard, C.T., Creaser, R.A., Lyons, T.W., Bekker, A., Poulton, S.W., Anbar, A.D., 2018. A model for the oceanic mass balance of rhenium and implications for the extent of Proterozoic ocean anoxia. Geochim. Cosmochim. Acta 227, 75–95.
Sperling, E.A., Knoll, A.H., Girguis, P.R., 2015a. The ecological physiology of Earth's second oxygen revolution. Annu. Rev. Ecol. Evol. Syst. 46, 215–235.
Sperling, E.A., Wolock, C.J., Morgan, A.S., Gill, B.C., Kunzmann, M., Halverson, G.P., Macdonald, F.A., Knoll, A.H., Johnston, D.T., 2015b. Statistical analysis of iron geochemical data suggests limited late Proterozoic oxygenation. Nature 523, 451–454.
Sperling, E.A., Carbone, C., Strauss, J.V., Johnston, D.T., Narbonne, G.M., Macdonald, F.A., 2016. Oxygen, facies, and secular controls on the appearance of Cryogenian and Ediacaran body and trace fossils in the Mackenzie Mountains of northwestern Canada. Geol. Soc. Am. Bull. 128, 558–575.
Them, T.R., Gill, B.C., Caruthers, A.H., Gerhardt, A.M., Gröcke, D.R., Lyons, T.W., Marroquin, S.M., Nielsen, S.G., Trabucho Alexandre, J.P., Owens, J.D., 2018. Thallium isotopes reveal protracted anoxia during the Toarcian (Early Jurassic) associated with volcanism, carbon burial, and mass extinction. Proc. Natl. Acad. Sci. 115, 6596–6601.
Tribovillard, N., Algeo, T.J., Lyons, T.W., Riboulleau, A., 2006. Trace metals as paleoredox and paleoproductivity proxies: an update. Chem. Geol. 232, 12–32.
Wang, L., Shi, X., Jiang, G., 2012. Pyrite morphology and redox fluctuations recorded in the Ediacaran Doushantuo Formation. Palaeogeogr. Palaeoclimatol. Palaeoecol. 333, 218–227.
Zhang, F., Xiao, S., Kendall, B., Romaniello, S.J., Cui, H., Meyer, M., Gilleaudeau, G.J., Kaufman, A.J., Anbar, A.D., 2018. Extensive marine anoxia during the terminal Ediacaran Period. Sci. Adv. 4, eaan8983.
Zhang, F., Xiao, S., Romaniello, S.J., Hardisty, D., Li, C., Melezhik, V., Pokrovsky, B., Cheng, M., Shi, W., Lenton, T.M., Anbar, A.D., 2019. Global marine redox changes drove the rise and fall of the Ediacaran biota. Geobiology 17, 594–610.